University of Amsterdam

MSc Physics

Advanced Matter and Energy Physics

Master Thesis

Harnessing singlet exciton fission to enhance silicon solar cells through direct charge-transfer

---

by

Koen van den Hoven

Stud.nr: 10677143

August 2018
60 ECTS
September 2017 - August 2018

1st Examiner:
Prof. Albert POLMAN

2nd Examiner:
Prof. Femius KOENDERINK

Supervisor:
Dr. Bruno EHRLER

Daily supervisor:
Moritz FUTSCHER

Abstract

Today silicon photovoltaic technology is dominating the global market with a total market share of over 95% and efficiencies reaching as high as 26.7%. However, conventional silicon cells have a hard efficiency limit of 29.4% (Auger constrained) and, therefore, the ever increasing efficiency of state-of-the-art silicon devices will soon come to a halt if we do not find ways to fight the major loss mechanisms in silicon photovoltaics. Singlet fission, an exciton multiplication mechanism in organic systems, might offer an effective approach to decrease thermalisation losses in silicon solar cells, accounting for 33% of the solar irradiation. In this report, we examine the potential of direct-charge transfer as a method to combine a singlet fission material with silicon. We simulate such a direct charge transfer device to find that, even for relatively realistic parameters, a 2% absolute improvement on the current record silicon efficiency can be achieved using either pentacene or tetracene, two well-known singlet fission materials. Optimised, novel, materials could help to increase the power conversion efficiency to values well over 30%, therefore improving on the single-junction Schockley-Queisser limit. However, to reach these efficiencies solutions are needed to drastically enhance the light absorption in the singlet fission layer. As a proof of principle, we fabricate two DCT architectures based on pentacene and silicon and study the performance of the devices. We find evidence of a internal quantum efficiency of about 25% from the pentacene layer. Further research is needed to confirm the singlet fission origin of this photocurrent.

Acknowledgements

First and foremost, I would like to thank Moritz Futscher for all the support throughout this project; you have been a great help and just a fantastic person to work with. I wish to thank Bruno Ehrler for all his advice and enthusiasm and the opportunity to carry out this internship. Special thanks to everyone that helped me in the lab: Jumin Lee for for sharing all his expertise on pretty much anything lab-related, Parisa Khoram for the help with the spatial EQE-system and Marc Duursma for being our go-to problem solver. This work would obviously not have been possible without our collaborators from the Helmholtz Zentrum in Berlin that have made the great silicon wafers that I used for my project. My final thanks go to the Hybrid Solar Cells group in general; thanks a lot for the welcoming atmosphere and all our interesting food and non-food related conversations.

Contents

1 Introduction **1**

2 Singlet fission basics and the potential of direct charge-transfer devices **5**

2.1 The Schockley-Queisser limit 5
2.2 The singlet fission process 7
2.3 Combining singlet fission with inorganic photovoltaics 8
2.4 Modelling a DCT singlet fission solar cell 11
2.4.1 The model 11
2.4.2 Realistic absorption 14
2.4.3 Ideal absorption 15
2.4.4 Device operations under realistic weather conditions 18
2.4.5 Assumptions 21
2.4.6 Conclusions 23

3 Towards experimental demonstration of direct charge-transfer in hybrid silicon/C_{60}/pentacene solar cells **25**

3.1 Device architectures 25
3.2 Methods 27
3.2.1 Device fabrication 27
3.2.2 Analytical methods 29
3.2.3 EQE model and fitting procedure 30
3.3 Results 32
3.3.1 PEDOT:PSS device performance 32
3.3.2 MoO_x/Al/Ag device performance 35
3.4 Discussion 37

4 Conclusion & outlook **41**

4.1 Conclusion 41
4.2 Outlook 42

Bibliography **45**

1 Introduction

Solar energy can become one of the most effective ways to address the world's growing energy demand in an environmentally friendly and sustainable manner. As the total photovoltaic (PV) deployment went from 180 GW in 2014 to a predicted 6000 GW in 2050 [19], continually falling electricity prices have raised awareness that solar energy can soon become the lowest-cost option for our future electricity supply. This rapid and wide-scale growth has been driven by the world's increased demand for renewable energy solutions, technological progress and the decreasing costs of PV modules. As a result of the continuing price reduction the module itself will have a falling share in the total costs of new solar electricity installations. Therefore, to further lower the costs of solar electricity two things are needed: 1) lower PV system costs, and 2) increased module solar-to-electricity efficiency, as this would increase the generated electrical power for the same system costs.

However, fundamental thermodynamic limits prevent the increase of the power conversion efficiency (PCE) of conventional solar cells. This maximum achievable efficiency is more commonly known as the Shockley-Queisser limit (SQ-limit) [34] and has been calculated to be 29.4% (Auger limited) in ideal silicon (Si) PV devices [33]. The gap between the current record PCE and the SQ-limit is closing rapidly with record efficiencies of 26.7% currently being reported in laboratory Si solar cells [46, 16]. Evidently, continuing to improve on current technology may not be the most effective strategy to improve solar-to-electricity PCE. Therefore, new approaches are needed to tackle the major loss mechanisms in conventional systems, making it possible to, eventually, reach beyond the single-junction SQ-limit.

The most substantial energy loss mechanism in all single junction systems is a process called thermalisation. Whether an incident photon has an energy equal to the semiconductor bandgap energy or above it, in both cases it will excite an electron-hole pair that will be collected at the exact same energy and the excess energy of the high-energy photon is lost as heat. For silicon solar cells thermalisation accounts for a 33% loss of the incident solar power (see figure 1.1) and, therefore, reducing these losses would greatly enhance the performance.

Singlet exciton fission (SF) [36] could be an effective approach to reduce these thermalisation losses [30]. In this process, two electron-hole pairs are created from

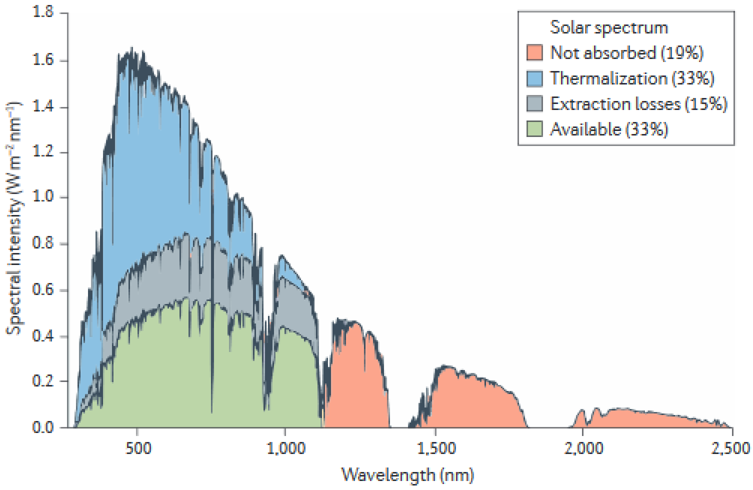

Fig. 1.1: The energy losses that lead to the SQ-limit in an ideal Si solar cell. The red part of the spectrum does not have enough energy to excite an electron to the conduction band. The blue region of the spectrum is converted into heat. In purple the effect of other extraction losses is shown. The final 33% of radiation energy is available for power conversion but the SQ-limit is reduced to 29.4% when Auger recombination is included. Figure adapted from Beard et al. [33].

a single high-energy photon. In organic chromophores, absorption of a photon will lead to the formation of a singlet exciton. In some materials this singlet exciton can share its excitation energy with a neighbouring ground-state molecule, in which case both are converted to triplet excitons with roughly half the singlet exciton energy. This process does not require a spin-flip and can occur very efficiently on very short timescales [36, 30]. Singlet fission could potentially reduce thermalisation losses in combination with a low bandgap semiconductor such as silicon. In this case low energy photons are absorbed in the silicon, generating one electron-hole pair per photon. High-energy photons can be captured in the singlet fission material which will result in the formation of, ideally, two excitons per photon. In such a hybrid device, the open circuit voltage is set by the low-bandgap material but for high-energy light *two* electrons are generated instead of one. As a result, the thermalisation losses are partly reduced and the potential PCE is increased. Detailed balance calculations suggest that singlet fission could increase the PCE of an ideal Si solar cell from 33% to over 40% (not taking into account Auger recombination) [36, 25].

There are multiple methods to make use of the singlet fission process in inorganic PV, and most of these methods intend to transfer the exciton into the inorganic cell [14, 41, 30]. However, efficient energy transfer has not yet been shown as these energy transfer methods require challenges related to device architectures, interfaces and surface treatment to be overcome before successful implementation. A promising alternative to these approaches would be direct charge-transfer (DCT). Instead of transferring the whole exciton to the base cell, this method aims to dissociate the triplet excitons into free charges using a donor-acceptor interface. Subsequently, the generated electrons and holes can be collected at their respective contacts. Exciton dissociation has been proven to be very efficient in pentacene/C_{60} systems [45, 35] and DCT also opens the possibility to below-bandgap triplet energies. Yet, this method has received little attention from the singlet fission research community and its potential still needs to be carefully examined.

In this report the basic concepts and mechanisms of the singlet fission process and the proposed hybrid device architectures will be introduced. Focusing on the direct charge-transfer approach, we will then discuss a model, based on the work of Futscher and Ehrler [12, 13, 14], describing the performance of hybrid singlet fission solar cells under standard and realistic operating conditions. Finally, experimental work will be shown where we attempt to find evidence of an additional photocurrent resulting from singlet fission in direct charge-transfer devices based on pentacene & silicon.

2 Singlet fission basics and the potential of direct charge-transfer devices

2.1 The Schockley-Queisser limit

One of the fundamental limitations on the performance of a photovoltaic device arises from the principles of detailed balance. A solar cell not only absorbs solar radiation but also exchanges thermal radiation with its surroundings. The rate of absorption of solar photons must match the rate of emission of photons by the cell in order for the amount of charges in the device to be constant in thermal equilibrium. We will, simplistically, consider a solar cell to be a two-level system of which the upper level (the conduction band) initially contains no electrons and the lower level (the valance band) is completely filled. The bandgap, E_g gives the energy difference between the two levels. We assume that all incident photons with $E > E_g$ are absorbed and excite an electron to the conduction band. The emission of a photon from the cell will be at the cost of an electron-hole pair and we assume both the solar cell and its ambient to behave like a black body (the spectral emission follows Planck's radiation law). If we also assume that no excited electrons are lost trough non-radiative processes we can now calculate the efficiency of this simplified solar cell. For a more elaborate explanation of the detailed balance equations we recommend *The Physics of Solar Cells* by Jenny Nelson [29].

We can start by calculating the current-density of a solar cell under illumination [29],

$$J(V) = J_G - J_R(V) = q\int_{E_g}^{\infty}\{\Gamma(E) - (b_e(E,qV) - b_a(E))\}dE \tag{2.1}$$

where J_G is the photo-generated current, J_R is the current lost by the recombination of generated charges, q is the elemental charge and Γ is the solar photon flux. Assuming a black body spectrum, b_e gives the radiated photon flux from the solar cell and b_a gives the absorbed photon flux from the ambient.

In order to calculate the PCE we need to know the incident power and the extracted power. The incident power is obtained by integrating the irradiance incident on the solar cell over the photon energy,

$$P_{incident} = \int_0^{\infty} E \cdot \Gamma(E) dE \tag{2.2}$$

The electrical power extracted from the solar cell is simply the product of the current with the voltage and thus, the PCE efficiency η can be written as,

$$\eta = \frac{VJ(V)}{P_{incident}} \tag{2.3}$$

Maximum efficiency is obtained when the extracted power is optimised and,

$$\frac{d}{dV}(VJ(V)) = 0 \tag{2.4}$$

The Schockley-Queisser limit refers to the maximum achievable solar-to-electricity power conversion efficiency of a single junction solar cell under the assumptions described above. In 1961 William Schockley and Hans-Joachim Queisser were the first to calculate this limit by detailed balance [34]. The main fundamental mechanisms limiting the efficiency of a solar cell under operation are:

Radiative recombination Any object with a nonzero temperature emits electromagnetic radiation. In order to radiate a thermal photon an electron in the conduction band has to recombine with a hole in the valence band; the potential energy is released in the form of a photon. The amount of energy lost in radiation for a solar cell at room temperature can be approximated by Planck's law and corresponds to about 7% of the incident energy.

Impedance matching The efficiency of a solar cell depends on its load, under a given illumination intensity there will be an optimum load resistance. Schockley and Quiesser call the ratio between the optimal power extracted and the theoretical maximum power ($V_{oc} \times J_{sc}$) the impedance matching factor, but it is more commonly known as the fill factor.

Spectrum losses Only photons with an energy equal to or higher than the bandgap energy can be absorbed and contribute to power generation. Furthermore, a photon with an energy above the bandgap will always produce an electron-hole pair with an energy equal to the bandgap energy; the excess energy will be lost in thermalisation.

Schockley and Queisser calculated the maximum achievable PCE to be 33.7% for a bandgap of 1.34 eV under standard AM1.5G solar irradiation. Si-based solar cells have a less favourable bandgap of 1.1 eV resulting in a SQ limit of 33%. Spectrum losses are responsible for the majority of lost power. For a Si solar cell all photons with an energy below 1.1 eV do not contribute, which corresponds to an energy loss of 19% [33]. Thermalisation is even more important and is responsible for an energy loss of about 33%. The final 15% is lost by radiative recombination and impedance matching. In figure 1.1, the magnitude of the different loss mechanisms for an ideal silicon solar cell under standard AM1.5G illumination are given.

Please note that the SQ-limit does not include material specific processes such as Auger recombination for silicon devices. When Auger recombination is also taken into account, the PCE limit of a silicon solar cell has been calculated to be 29.4% [33].

2.2 The singlet fission process

In organic semiconductor materials there is no such thing as a valence and conduction band. Instead, the material consists of molecules with orbitals that have different electronic energy levels. Each orbital can contain two electrons of opposite spin because of Pauli's exclusion principle. When a molecule absorbs an incident photon with sufficient energy, one of these electrons can be excited from the highest occupied molecular orbital (HOMO) to the lowest unoccupied molecular orbital (LUMO). The resulting state is the first excited singlet state (S_1), it is a spin-singlet state because both electrons still have opposite spin.

Singlet fission is a process where a spin-singlet state ($S = 0$) is converted to two spin-triplet states ($S = 1$), via a spin-allowed process (figure 2.1). The process can occur if the energy of the lowest lying singlet exciton (S_1) is twice that of the lowest lying triplet exciton (T_1) (some molecules even show singlet fission when the combined triplet-energy is slightly higher than that of the singlet exciton, as is the case in tetracene). Being a spin-allowed process, singlet fission can occur on ultra-fast timescales, outcompete radiative decay and reach a near-unity efficiency in some materials (e.g. pentacene).

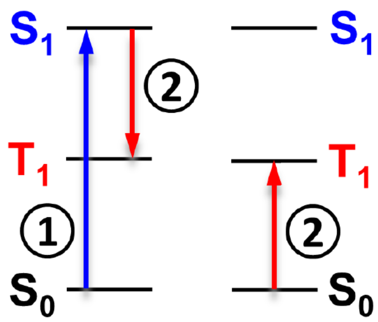

Fig. 2.1: The singlet fission process. The picture shows the energy levels for two molecules. The molecule on the left is photo-excited to the spin-singlet S_1 state (1) and, subsequently, the energy is distributed over the two molecules; creating a spin-triplet state on each site (2). Figure adapted from Liebhaber et al. [26].

The most common description of the singlet fission process was proposed by R. C. Johnson and R. E. Merrifield in 1970 [23]. The kinetic model, including multiple rate constants, is given by:

$$S_1 + S_0 \underset{k_{-1}}{\overset{k_1}{\rightleftarrows}} (TT) \underset{k_{-2}}{\overset{k_2}{\rightleftarrows}} T_1 + T_1 \tag{2.5}$$

where S_0 is the ground state and TT corresponds to a pair of spin-correlated triplet excited molecules. For an efficient singlet fission process the forward rate constants have to outcompete the backward, triplet fusion, rate constants. Please note that loss channels such as radiative singlet decay and triplet-triplet decay are not included in this simplified description. The exact dynamics of the singlet fission process and the role of the TT state have been studied extensively and are still under debate [36]. A more elaborate discussion of the singlet fission kinetics lies beyond the scope of this work.

In some materials, e.g. pentacene and tetracene, singlet fission quantum yields close to 200% and long lived triplet states in the order of nano- to microseconds have been reported [44, 36, 35]. In these materials the singlet fission rate outcompetes other processes such as radiative and non-radiative decay, and intersystem crossing.

2.3 Combining singlet fission with inorganic photovoltaics

Silicon based PV technology accounted for roughly 95% of the total production in 2017 and its market share only seems to increase [15, 37]. With current PCE's of up to 26.7% [16, 46] approaching the Auger-limited Schockley-Queisser limit, fighting thermalisation losses is becoming ever more important to increase the performance of this dominating technology. Therefore, using singlet fission to reduce the thermalisation losses of silicon solar cells is an interesting idea worth investigating.

Essentially, there are two ways to make use of the singlet fission process in inorganic PV: using energy transfer or charge-transfer. In the first case the triplet exciton is transferred to the bulk of the silicon cell. This is challenging because the excited electron in a triplet exciton cannot decay directly (radiatively) to the ground state and therefore long-range Förster resonance energy transfer [10] is not possible. This can be partially solved by transferring the triplet exciton to inorganic quantum dots via Dexter resonance energy transfer (a shorter range energy transfer process) [8]. Recent studies have investigated the possibility to transfer the exciton energy from the nanoparticles into silicon via Förster resonance energy transfer [41] or by the emission of a photon [14], but the predicted efficiency of energy transfer remains relatively low. In principle, energy transfer can also be accomplished by direct Dexter energy transfer from the singlet fission material into silicon. This would require wave-function overlap between the singlet fission material and the inorganic compound and therefore needs the molecules to be in very close proximity to the surface. Using a functionalised silicon surface with covalently bonded organic molecules to enhance wave-function overlap with the singlet fission material might be a viable approach to accomplish energy transfer [7], but remains unproven. All described energy transfer methods require challenges related to device architectures, interfaces and surface treatments to be overcome before successful implementation.

A promising alternative route would be to not transfer the whole exciton to the base cell but rather separate the triplet exciton into free charges using a donor-acceptor heterojunction. Subsequently, the electron and hole can be transported to their respective contacts. This transfer approach is known as direct charge-transfer (DCT). It has been shown that pentacene/C_{60} interlayers can successfully separate charges within several nanoseconds after excitation [45, 11] and can be used to fabricate solar cells with external quantum efficiency (EQE), the number of collected charges per incident photon, well above 100% [6]. In contrast to series-tandem devices, there is no need for current-matching in DCT cells and it opens the possibility to use singlet fission materials with triplet exciton energies below the silicon bandgap of 1.12 eV. This transfer method has received little attention from the scientific community and, therefore, little is known about the challenges to overcome. Probably, the major obstacle for efficient charge-transfer is to minimise band offsets and energy losses from recombination across the organic-inorganic interface.

A DCT cell can consists of a low-gap semiconductor, in our case silicon, covered with a singlet fission material and a acceptor layer. The high energy light will be absorbed in the singlet fission material and the low energy light is absorbed in the silicon wafer.

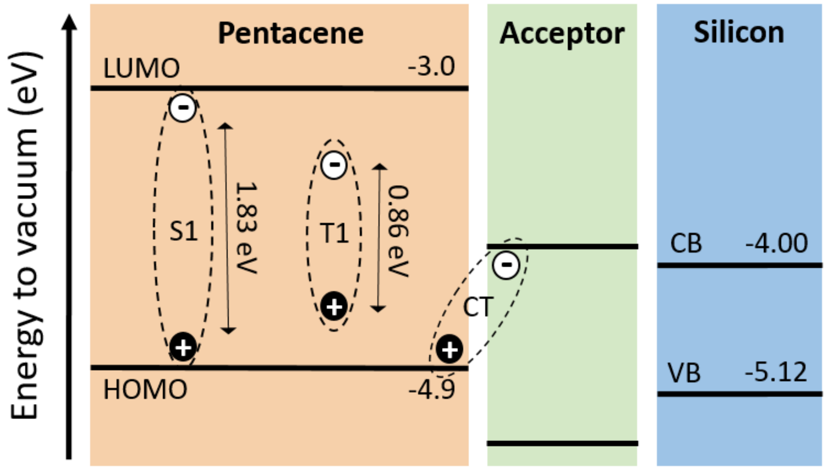

Fig. 2.2: Energy diagram for the essential materials in a DCT cell using pentacene as the singlet fission material and silicon as the bottom layer.

If we take pentacene to be the singlet fission material the energy diagram will look like displayed in figure 2.2. Photons absorbed in the pentacene layer will excite an electron to the S_1 state, and because there is a strong binding energy between the electron and the hole, the energy of the singlet exciton (1.83 eV) will be less than the HOMO-LUMO offset. This singlet exciton quickly decays (on 80 ps timescales [21, 45]) into two triplet excitons with an energy of 0.86 eV. These excitons can move from molecule to molecule via Dexter transfer until they find the acceptor interface. Often fullerenes are used for the electron acceptor layer in singlet fission devices [6, 5, 24]. These fullerenes are strong electron acceptors with a LUMO-level below the LUMO-level of most singlet fission materials, as a result the electron will be pulled into the fullerene layer and form a charge-transfer (CT) state. This CT state is bound to the interface so the electron hole pair can either recombine or dissociate. As it turns out, in pentacene/C_{60} systems exciton dissociation is very fast, occurring on sub-100 fs timescales, outcompeting recombination processes [45, 6].

The dissociated charges now have to find their respective contacts. The hole can diffuse trough the pentacene layer to the top contact and the the electron has to be transferred to the silicon layer to ultimately find the back contact. The electrons that are generated in the silicon can easily find the same back contact but the holes have to diffuse trough the singlet fission material. All these processes still have to be shown to be possible.

2.4 Modelling a DCT singlet fission solar cell

In this section we will describe a model, based on previous work of Futscher & Ehrler [12, 13, 14], and extend it to simulate the performance of a hybrid singlet fission solar cell under realistic operating conditions using the direct charge-transfer method. Although there is no evidence yet of a working device with this architecture the model provides insight into the significance of several physical parameters such as the singlet- and triplet-energy of the fission material, charge separation efficiency, charge diffusion efficiency and losses due to absorption. The results of the model can be used to identify the main issues restraining the potential of current state-of-the-art technology and help to direct future research.

2.4.1 The model

In the detailed-balance calculations described in chapter 2.1 all recombination is radiative and all photons above the bandgap are absorbed and generate current (EQE = 1). The model described here is an extension of the detailed balance limit to include non-radiative recombination, Auger recombination, shunt resistance and series resistance. The total current density is then described by

$$\begin{aligned} J(V) = J_G(Spectrum, EQE) - J_R(V, T, R_s) \\ - J_{NR}(V, T, R_s) - J_A(V, T, R_s) - \frac{V + JR_s}{R_{sh}} \end{aligned} \tag{2.6}$$

where J_G is the generated photocurrent density, J_R the radiative recombination current density, J_{NR} is the non-radiative recombination current density and J_A gives the Auger recombination current density. V is the voltage, T is the temperature and the series and shunt resistances are given by R_s and R_{sh}, respectively. The generated current and recombination current terms now include losses from series resistance. The temperature dependent Auger recombination term is calculated according to Dziewior & Schmid [9]. The temperature dependence of the intrinsic charge carrier population and the Si bandgap are accounted for [42, 28]. The magnitude of J_{NR} together with the series and shunt resistances are left as fitting parameters. For a more detailed description of the model we refer to the work of Futscher & Ehrler [13].

To simulate a silicon cell under changing operating conditions the model is fitted to the current-voltage characteristic of that particular device where we use the reported EQE-spectrum to account for optical losses in the solar cell. After the determination of the fitting parameters the light-spectrum and the temperature can be changed while the model still accurately predicts the current-voltage characteristic of the device, see figure 2.3.

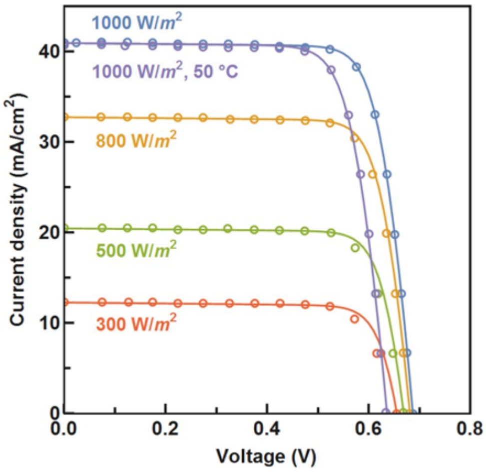

Fig. 2.3: Measured current-voltage characteristics (circles) of a commercially available Sunpower solar cell with an efficiency of 22.5%. The model is fitted to the measurements taken under standard test conditions (AM1.5G, 1000W/m^2, 25°C). When the temperature or the irradiance is changed the model still fits the measurements with reasonable accuracy. Figure adapted from Futscher et al. [12].

We expand on this model by simulating a singlet fission material with an acceptor layer on top of the modelled silicon device (see figure 2.5). The singlet fission layer absorbs photons that are dissociated into free charges at the acceptor interface. The number of collected charges for every absorbed photon is regulated by a certain overall quantum efficiency (*QE*) which can be decomposed as

$$QE = T_1 \cdot IQE = T_1 \cdot \eta_{SF} \cdot \eta_{CS} \cdot \eta_{Coll} \tag{2.7}$$

where T_1 gives the transmission (on a scale of 0 to 1) trough the top contact and hole transporting layer and IQE gives the internal quantum efficiency (the number of collected electrons per absorbed photon) of the singlet fission material (on a scale of 0 to 2). The IQE is a result of three efficiencies, η_{SF} gives the singlet fission efficiency (on a scale of 0 to 2), η_{CS} gives the charge separation efficiency (on a scale of 0 to 1) and η_{Coll} gives the efficiency at which the charges are collected (on a scale of 0 to 1).

Using an absorption spectrum measured for a 50 nm layer of thermally evaporated pentacene and tetracene, we can approximate the the absorption of the materials, and thus the number of absorbed photons, for an arbitrary layer thickness using the Beer-Lambert law [38]. As an example, figure 2.4 shows the transmission spectrum for a pentacene layer of a given thickness when exposed to the standard AM1.5G solar spectrum. The "missing" part of the spectrum is absorbed by the pentacene

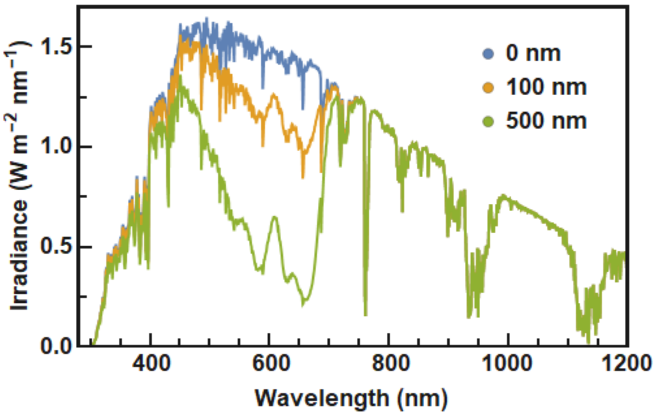

Fig. 2.4: The transmission spectrum for a pentacene layer of 0, 100 and 500 nm in thickness when exposed to the standard AM1.5G solar spectrum. The absorption of a pentacene layer of a given thickness was calculated using the Lambert-Beer law and the absorption spectrum of a 50 nm layer of thermally evaporated pentacene.

layer and the number of photons absorbed times the *QE* will give the number of electrons that are added to the generated photocurrent of the silicon wafer. The silicon layer will receive the solar spectrum minus the light that is absorbed by the singlet fission layer and multiplied by the transmission coefficient $T = T_1 \times T_2$ to account for parasitic absorption and reflection losses in the contacts/hole transport layer (T_1) and in the singlet fission/electron acceptor layer (T_2). We assume that the hybrid device will have a series resistance twice as high as the silicon cell to account for the the added material layers.

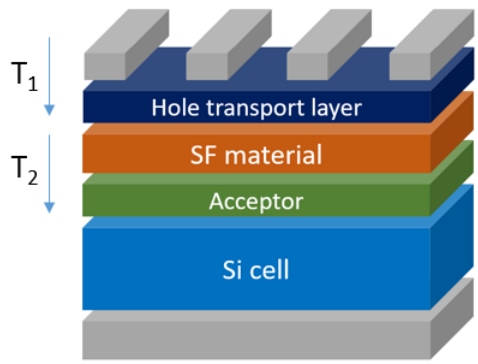

Fig. 2.5: The basic structure of a direct charge-transfer hybrid singlet fission device. T_1 gives the transmission to the singlet fission material to account for reflection and absorption in the top contact and hole transporting layer, T_2 gives the transmission trough the singlet fission and electron acceptor layer.

It is important to note that if the triplet-energy of the singlet fission material is smaller than the bandgap of silicon, e.g. pentacene , the overall energy offset between the electron and hole contact of the solar cell will have to be reduced. This means that, if the energy levels of the triplet exciton and the conduction band of silicon are perfectly aligned, there will be a reduction in the energy offset equal to $\Delta E = E_g - E(T_1)$ where E_g is the bandgap of silicon and $E(T_1)$ is the triplet exciton energy. For pentacene there will be a voltage penalty corresponding to $\Delta E = 0.26$ eV. For tetracene ($E(T_1)$ = 1.25 eV) there is no voltage penalty.

2.4.2 Realistic absorption

We will simulate the performance of a tetracene and a pentacene based DCT device. This makes for an interesting comparison for three reasons: 1) tetracene and pentacene are the most common and well-studied singlet fission materials, 2) singlet fission in tetracene is endothermic by 75 meV, whereas pentacene is exothermic by about 50 meV, 3) pentacene will suffer from a voltage penalty because its triplet-energy is below that of the silicon bandgap, the tetracene triplet-energy is well above the silicon bandgap.

For the silicon base cell the current record efficiency device with an efficiency of 26.7% [16, 46] is used. If we, optimistically, assume a transmission coefficient of 95% to the silicon wafer, a QE of 2 and a singlet fission material thickness of 500 nm, we can simulate the JV-characteristics for a tetracene (figure 2.6a) and a pentacene (figure 2.6b) hybrid solar cell under standard test conditions (AM1.5G spectrum, 1000W/m^2 incident power, 25°C). The efficiency of the full device is calculated from the current-voltage characteristic, also for different parameter sets. In figure 2.6c,d the efficiency as a function of the QE and layer thickness is shown for a tetracene and pentacene based device.

The efficiency profile in figure 2.6 of both devices looks rather similar. Obviously, the tetracene based cell with a maximum efficiency of 29.1% (QE = 2, Thickness = 500 nm, T = 0.95) outperforms the pentacene device (26.8 % under the same conditions), because it has a triplet-energy of 1.25 eV and therefore does not suffer from a voltage penalty. However, it is interesting to see that the pentacene device shows a larger increase in efficiency when moving to higher QE and thickness parameters, as indicated by the denser contour lines in figure 2.6. This is due to the fact that it has a lower singlet-energy (1.86 eV) compared to tetracene (2.35 eV) and therefore can absorb photons over a larger part of the solar spectrum. Because pentacene absorbs more photons it adds a larger current to the silicon cell (see figure 2.6a, b) and benefits more from an increase in quantum efficiency or layer thickness.

Note that efficiencies surpassing the record PCE of a silicon solar cell (depicted by the solid black line in figure 2.6) are only achieved for a tetracene layer thickness above a $\sim$100 nm and a pentacene layer thickness above $\sim$500 nm. The triplet exciton diffusion length in polycrystaline films of, respectively, tetracene and pentacene is estimated to be 0.4 ±0.2 µm [43] and approximately 40 nm [39]. In reality, films

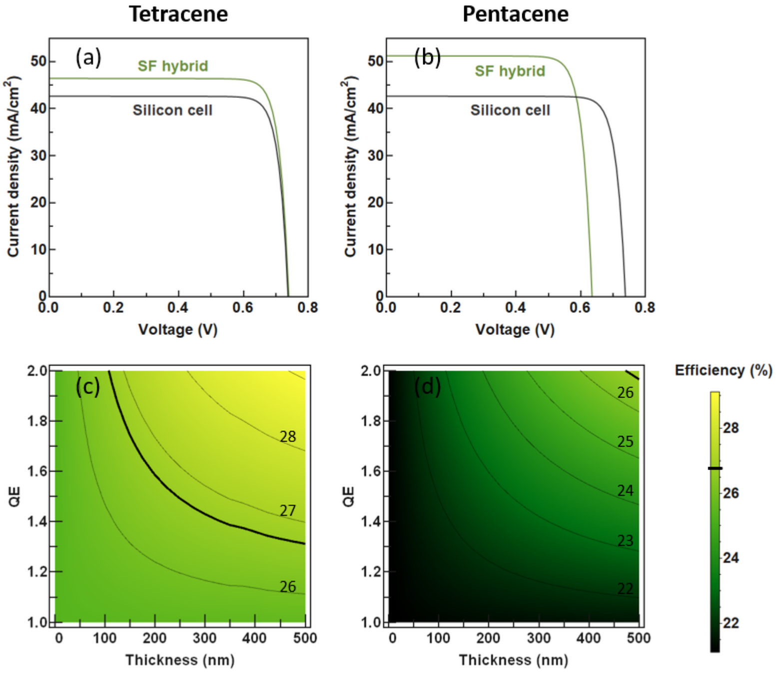

Fig. 2.6: **(a, b)** Current density of a hybrid singlet fission solar cell (solid green lines) with a tetracene (a) and pentacene (b) layer of 500 nm calculated for a quantum efficiency of 2 and 95% transmission to the silicon wafer. The record silicon device without a singlet fission layer (black solid line). **(c, d)** The simulated efficiency of the tetracene (c) and pentacene (d) device as a function of the layer thickness and the quantum efficiency. The solid black line gives the record PCE for a silicon solar cell (26.7%).

thicker then the triplet exciton diffusion length will suffer from a significantly lower QE because a large part of the triplets will be lost before the acceptor interface is reached. Therefore, the silicon record PCE might still be within reach for a tetracene based DCT device (a PCE of 26.7 is reached for a QE of 1.6 in combination with a thickness of 200 nm, which is still relatively realistic) but for pentacene even thicknesses well beyond the triplet exciton diffusion length are not sufficient to beat the record silicon device.

2.4.3 Ideal absorption

Setting aside the issues regarding low absorption and limited diffusion length (we will address these challenges in the conclusion of this section), the realistic absorption simulation shows us that the efficiency of a pentacene DCT device increases faster for increasing thickness, despite the voltage penalty associated with its below E_g triplet exciton energy. This observation leads us to an interesting question: what would be the most ideal set of exciton energies in a singlet fission material for future devices? Lower singlet energies mean that a bigger fraction of the spectrum can be used for singlet fission whereas a lower triplet-energy leads to a higher voltage penalty. To find out we will simulate a device assuming perfect absorption below the singlet exciton energy and a triplet exciton energy of exactly half E(S_1). Plotting the efficiency as a function of the quantum efficiency and the singlet-energy yields the graph shown in figure 2.7 (for T = 0.95).

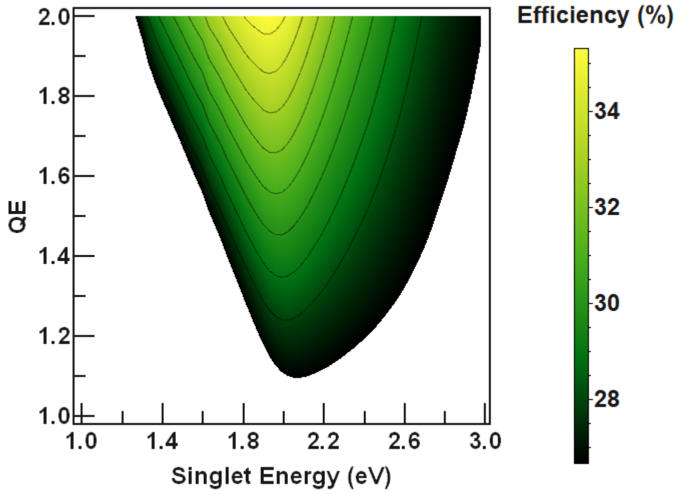

Fig. 2.7: The efficiency of a DCT singlet fission cell (T = 0.95) with full absorption plotted as a function of the quantum efficiency and the singlet-energy. The triplet exciton energy is set to half the singlet exciton energy. Only efficiencies greater than that of the silicon base cell (26.7%) are shown.

The results are striking, a maximum PCE of a staggering 35.06% is achieved for an ideal singlet fission layer (QE = 2) with a singlet exciton energy of only 1.92 eV. Remarkably, this maximum efficiency gain, of over 8% absolute, is achieved for a triplet-energy that is lower than the bandgap energy of silicon (1.12 eV). Furthermore, a DCT architecture improves on the bare silicon cell for a large range of singlet energies and fairly low QE. Efficiencies of over 30% can be achieved for a QE of 1.5 (with the right singlet fission material).

The "shape" of the graph in figure 2.7 can be explained by careful examination of the different contributions to the photocurrent and open circuit voltage. In figure 2.8a the PCE for QE = 1.7 and T = 0.95 is shown. If we integrate the solar flux that can be absorbed by the ideal absorbing singlet fission material and the silicon layer (E_g = 1.12 eV) in a DCT architecture we find the photocurrent available to both cells. We can correct for the quantum efficiency and transmission by multiplying the singlet fission contribution by 1.7 and the silicon contribution by 0.95 to get the short circuit current of both layers, as shown in figure 2.8b. The open circuit voltage as a result of the triplet-energy is shown in green. Keeping in mind that $\eta \propto V_{oc} \times J_{sc}$, it is easy to see that these three different contributions will give rise to the efficiency profile in figure 2.8a.

Now that we understand how to explain this efficiency profile we can conclude that the optimal singlet exciton energy is determined by the ratio between the silicon and singlet fission contributions in figure 2.7. A lower silicon contribution (as a result of lower transmission or a lower efficiency cell) or a higher singlet fission contribution (as a result of a higher QE) results in a maximum efficiency at lower singlet energies and a higher silicon contribution (as a result of higher transmission or a better cell) or a lower singlet fission contribution (as a result of a lower QE) results in a maximum efficiency at higher singlet energies.

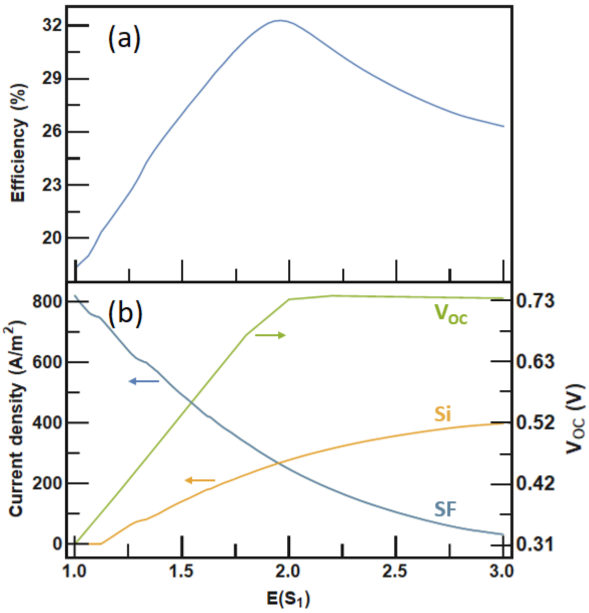

Fig. 2.8: (a) The calculated efficiency of a DCT cell for QE = 1.7 and T = 0.95. (b) The available current density for the SF material and the Si layer for changing singlet exciton energy (the values have been multiplied by 1.7 and 0.95 respectively to account for the QE and T of panel (a)). In green: the open circuit voltage of the hybrid device for changing singlet exciton energy.

In figure 2.9 the dependency of the efficiency on the transmission and singlet-energy is shown for QE = 1.7. It shows that for a lower transmission the optimal singlet-energy will shift to even lower energies, which is expected if the silicon photocurrent in figure 2.8b is lowered. The efficiency turns out to be heavily dependent on the transmission, for every 5% decrease in in transmission the efficiency drops by roughly one percent absolute. For low transmission values (< 0.8) $E(S_1)$ needs to lie within a 0.5 eV margin to still improve on the record silicon device.

In the above calculations we have assumed that $E(S_1) = 2E(T_1)$ but this does not have to be the case. There are singlet fission materials that are endothermic. This means that the triplet-energy is more than half the singlet-energy. Tetracene for example forms two triplets excitons of 1.25 eV from a singlet exciton of 2.35 eV and thus is endothermic by 1.25 eV - $\frac{2.35 \text{ eV}}{2}$ = 75 meV per triplet. More recently, Tabachnyk et al. [40] have shown that there can also be an entropic energy gain

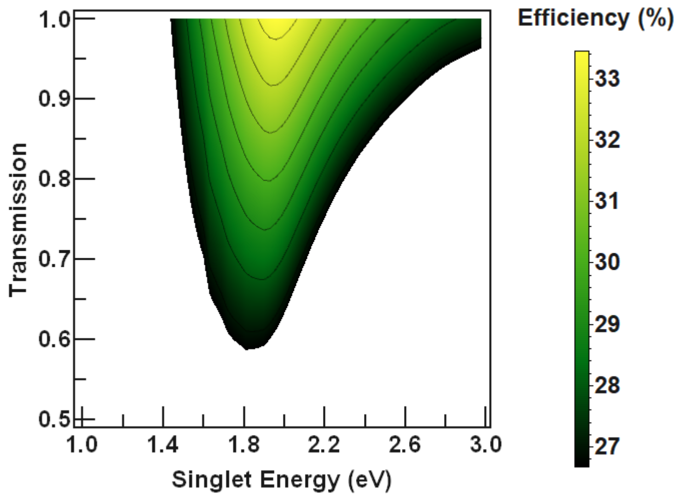

Fig. 2.9: The efficiency of a DCT hybrid singlet fission cell (QE = 1.7) with perfect absorption plotted as a function of the transmission to the silicon layer and the singlet-energy. The triplet exciton energy is set to half the singlet exciton energy. Only efficiencies greater than that of the silicon base cell (26.7%) are shown.

from charge separation, in their study they investigated a multistack of C_{60} and pentacene layers and found efficient and long-range charge separation within 50 ps from the formation of the charge transfer state, despite a Coulombic barrier which they estimate to be 220 meV.

To see the potential effect of an energy gain in a DCT cell (again, assuming that the energy levels of the triplet/acceptor are perfectly aligned) the efficiency for the optimal singlet-energy with an energy gain of 100 and 200 meV is shown in figure 2.10, again using a transmission of 95%. For a 200 meV energy gain the efficiency rises to a remarkable 42.8% at the maximum quantum efficiency of 2. All optimised singlet fission materials reach efficiencies over the Auger limited SQ-limit for silicon. The figure also illustrates the increase in efficiency of a pentacene based DCT device for increasing QE, surpassing tetracene at QE = ~1.8 (this crossover will shift to the left when the transmission is decreased according to the analysis following figure 2.8). We note that endothermic singlet fission materials often show slower and less efficient triplet generation, so in reality the maximum achievable QE is probably lower for more endothermic materials.

2.4.4 Device operations under realistic weather conditions

The model can also be used to simulate the performance under realistic weather conditions. To this purpose, we use the spectral and temperature data over an entire year (2015) as measured by the Utrecht Photovoltaic Outdoor Test Facility in the Netherlands [32]. These simulations will give information about how hybrid DCT

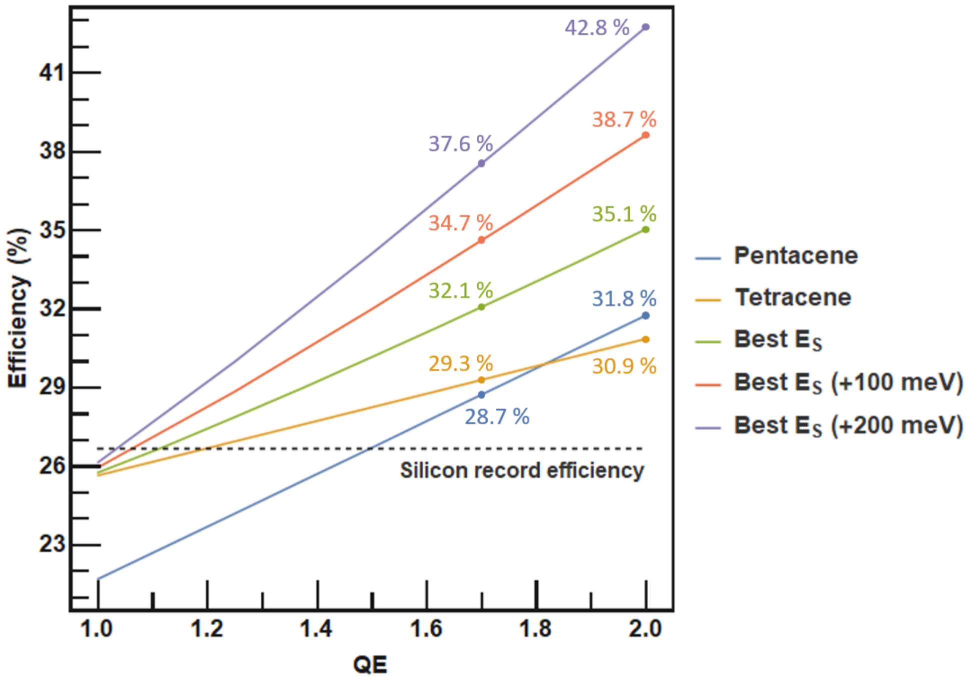

Fig. 2.10: The efficiency of DCT singlet fission devices for increasing quantum efficiency with a transmission of 95%. Pentacene (blue): E_S = 1.83 eV, E_T = 0.86 eV. Tetracene (orange): E_S = 1.83 eV, E_T = 0.86 eV). The other lines show the maximum efficiency reachable by varying E_S for a given QE. $E_T = \frac{1}{2}$ E_S (green), $E_T = \frac{1}{2}$ E_S + 100 meV (red) and $E_T = \frac{1}{2}$ E_S + 200 meV (purple). Efficiencies are given for QE = 1.7 and QE = 2.0.

cells under non-standard conditions, such as low irradiance or high average photon energy, and ultimately provide insight in the feasibility of real world deployment.

It is also interesting to see how the efficiency gain compared to the silicon base cell changes with the efficiency of the base cell. From previous work by Futscher et al. [14] we know that for silicon based tandem solar cells, the most popular approach to reach efficiencies beyond the SQ-limit, the absolute efficiency gain decreases for silicon base cells of increasing quality. In figure 2.11a the average PCE has been plotted for different singlet fission materials using silicon base cells of increasing recorded efficiencies. The simulated singlet fission materials are the same as in figure 2.10: pentacene ($E(S_1)$ = 1.83 eV, $E(T_1)$ = 0.86 eV), tetracene ($E(S_1)$ = 2.35 eV, $E(T_1)$ = 1.25 eV), optimal singlet exciton energy ($E(S_1) = 2E(T_1)$ = 1.967 eV, optimal singlet exciton energy with an energy gain of 100 meV ($E(S_1) = 2E(T_1)$ - 200 meV = 1.738 eV, optimal singlet exciton energy with an energy gain of 200 meV ($E(S_1) = 2E(T_1)$ - 400 meV = 1.527 eV)). Transmission is once again set to 95% and the QE in all devices is 1.7. For the optimal $E(S_1)$ devices, the singlet-energy has been optimised under standard test conditions using the silicon record cell as the base cell. The silicon cell efficiency on the x-axis is the calculated average efficiency over the entire year.

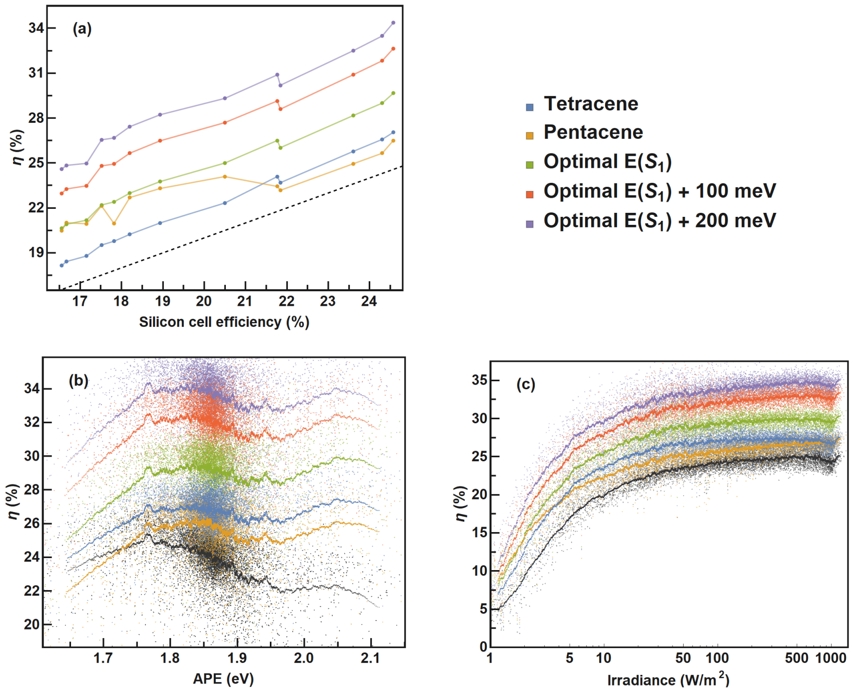

Fig. 2.11: Realistic conditions simulations of five different singlet fission materials used in hybrid devices. The temperature and spectra used for these simulations where measured in 2015 by the Utrecht Photovoltaic Outdoor Test Facility in the Netherlands [32]. (a) The efficiency of the DCT devices for silicon base cells of increasing PCE. (b,c) The efficiency of the DCT devices based on the record efficiency silicon solar cell against the average photon energy (b) and against the irradiance (c) of the measured spectra. The record silicon cell performance is given in black. The solid lines give a moving average on the data.

Clearly, the efficiency gain (with respect to the silicon base cell) is relatively constant for the different silicon devices and for the different singlet fission materials. The exception is pentacene, these devices show an efficiency gain of almost 4% absolute for the worst silicon cell and less than 2% absolute efficiency gain for the best silicon base cells. We can, again, explain this seemingly odd behaviour with the analysis in figure 2.8. A worse base cell leads to lower optimum singlet energies; the optimum energy lies fairly close to the pentacene $E(S_1) = 1.83$ eV for the lower silicon efficiencies and then drifts towards higher optimal $E(S_1)$. As expected from figure 2.10 the pentacene efficiency ends just below the tetracene device efficiency for the record silicon solar cell. Due to differences in the properties of the silicon cells (EQE, resistances etc.) there is some variation in the efficiency gain of the DCT devices, silicon cell 5 for instance has very poor EQE below 1.8 eV which causes the pentacene device to perform much worse when compared to the higher $E(S_1)$ singlet fission materials. For details on the silicon devices used in this simulation we refer to the work of Futscher et al. [14].

In figure 2.11b and 2.11c we show the PCE of the silicon record cell in combination with the different singlet fission materials for all spectra in the dataset. Figure 2.11b plots the efficiency against the average photon energy (APE), the black dots give the PCE of the bare silicon solar cell. All DCT devices perform better compared to the bare silicon cell. Not only are they more efficient, the device efficiency is also more stable under average and high average photon energy. This is expected since in the bare silicon cell a large part of the irradiated power would be lost in thermalisation, especially at higher APE, the singlet fission layer makes better use of the high energy light and helps to reduce thermalisation losses. Figure 2.11c gives the PCE as a function of the irradiance. All devices show similar behaviour with respect to the silicon solar cell. The singlet fission layer simply adds a current to the silicon device without significantly changing the silicon cells dependence on the irradiance.

The DCT devices seem to be more stable in changing weather conditions compared to two-terminal tandem solar cells. The need for current-matching between the top and bottom cell in these devices would lead to a significant decrease in efficiency for APEs deviating from standard test conditions. A change in the spectral irradiance distribution would lead to a discrepancy in the generated current between the two sub-cells. Being series connected, the efficiency decreases as the generated current is limited to the that of the cell producing the lowest current. A perovskite-silicon two-terminal tandem cell will also show a greater dependency on the irradiance because the total shunt resistance of the device will be the sum of both sub-cells and at low intensity this causes a significant drop in efficiency compared to the silicon cell alone. For a more elaborate discussion of these effects we refer to Futcher at al. [14].

2.4.5 Assumptions

Most of the simulation shown in this report have been performed using QE = 1.7 and T = 0.95. These numbers are very optimistic and currently far out of reach. However, we argue that these parameters are not entirely out of scope:

Quantum efficiency The quantum efficiency is a combined parameter, see equation 2.7. Singlet exciton fission efficiency can be very high for a lot of materials. In pentacene for example it is nearly 200%. Charge separation efficiencies in pentacene/C_{60} interlayers can also approach near unity efficiency (say 95%). If we also assume a 95% chance of collecting the charges at the contacts and a light transmission to the singlet fission material of 95%, we get a QE of $\sim$1.71.

Transmission High-performance front-contacted silicon solar cells reach close to 100% transmission to the silicon wafer. Most of the transmission is not lost through absorption in the top layer but from reflection from the layers covering the silicon. We argue that a working DCT cell will only have one or two interfaces more and with a optimised cell design the transmission to the silicon layer in DCT cells should be able to reach high values as well. To illustrate this point we compare the reflection from a layer of SiN (a common anti-reflection coating) on silicon to that of a simplistic DCT device, PEDOT:PSS/Pentacene/Si. The thickness of the SiN layer is optimised to 70 nm to maximise the generated current in the silicon under AM1.5G illumination. The PEDOT:PSS layer, a common hole-selective contact material, was set to 50 nm (this is optimistically thin, but not impossible) and the pentacene layer was set to 100 nm (educated guess for the thickness of the organics in a future DCT device). Using the code based on the TransferMatrix model developed in the McGehee group at Stanford University [1], ignoring absorption in the layers (i.e. only taking into account the n-values of the materials involved), the reflection from these stacks is calculated, see figure 2.12. As illustrated by the figure, the DCT cell reflection is much higher in the 400-700 nm wavelength range but reaches values below 10% for higher wavelengths. Arguably, the reflection in the lower wavelength regime is not very important for the performance of the silicon cell in a DCT architecture as this part of the solar spectrum will be absorbed by the singlet fission material. Textured surfaces can lower the reflection from both material stacks to even lower values, and therefore, a transmission parameter of 0.95 could lie within reach, at least for wavelengths above 700 nm.

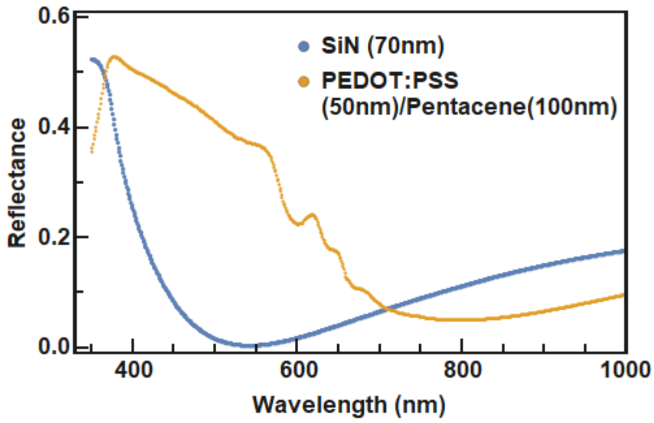

Fig. 2.12: The simulated reflection from a SiN layer (70 nm) and a PEDOT:PSS(50 nm)/pentacene(100 nm) stack on a silicon wafer of infinite thickness. The calculations have been performed using a TransferMatrix model [1] and ignoring the extinction coefficient of the materials involved.

All calculations have been performed with a series resistance of the organic layers equal to that of the silicon cell used (R_s(total) = 2 R_s(silicon)). The shunt resistance was not altered from the fitted value of the silicon base cell. We further assumed perfect alignment between the T_1-state and the conduction band of silicon. In practise this will be very hard to realise. If there is an energy offset, due to imperfect alignment, this will not necessarily result in a loss in efficiency. Only when the triplet-energy minus the energy offset drops below the silicon bandgap there will be a voltage penalty, and the efficiency will be reduced. Finally, the fact that trap states, for instance at the hybrid organic/inorganic interface, can also lead to a reduction in voltage was neglected. For all these reasons, the efficiencies given in this report should be viewed as an upper limit to the performance under the stated transmission and quantum efficiency parameters.

2.4.6 Conclusions

From the simulations discussed in the previous sections we draw a few, perhaps unexpected, conclusions.

Optimal exciton energies are lower than expected
It is commonly accepted that singlet fission materials with triplet exciton energies above the inorganic bandgap (e.g. tetracene) will outperform materials with a lower triplet and singlet-energy (e.g. pentacene) in DCT devices. This turns out to be a misconception; although there is a voltage penalty accompanied by lower triplet-energy materials, they will also absorb a larger part of the solar spectrum and therefore generate a greater current. As it turns out, the optimal singlet fission material to be used in a DCT architecture is one with a singlet exciton energy between 1.8 and 2.0 eV (depending on the transmission, quantum efficiency and silicon cell PCE, see figure 2.7 and 2.9). In theory a higher triplet exciton is beneficial (figure 2.10) but more endothermic materials often show slower and less efficient singlet fission which will reduce the quantum efficiency and therefore the overall device performance.

Absorption is vital
Absorption is key to high efficiency hybrid singlet fission solar cells. Comparing the maximum efficiency calculated using the realistic and ideal absorption model shows a 1.2% absolute increase for tetracene (realistic (500 nm): 28.1%, ideal: 29.3%) and a 3.4% absolute increase for pentacene (realistic (500 nm): 25.3%, ideal: 28.7%). Reaching full absorption below the singlet exciton energy is still a big challenge. Singlet fission materials generally show close to zero absorption between the S_1 and S_2 states which means that thicker layers will not be sufficient (on top of the issues regarding the exciton diffusion length).

A solution could be to combine two different singlet fission materials that have no (or very little) overlap in their S_1 absorption peaks and therefore collectively absorb over a broader range of the solar spectrum. A combination of tetracene (absorbing between 400 and 550 nm) and pentacene (absorbing between 550 and 670 nm) for example could absorb over a broad energy range, but for these materials the layers still have to be very thick to absorb an appreciable amount of the irradiation; as illustrated in figure 2.13 it would require a 1 μm layer of tetracene followed by a 1 μm layer of pentacene to absorb about 92% of the solar irradiation with a wavelength between 400 nm and 670 nm. To absorb 73% of the light in this range two 500 nm layers are needed. The triplet exciton diffusion length for these materials is not large enough to allow layers of such thickness without severely compromising the quantum efficiency of singlet fission in the device.

Another possibility would be to to add a strongly absorbing organic layer or nanostructure (e.g. quantum dots) on top of the singlet fission material. This absorber should have a $E(S_1)$ or E_g slightly greater than $E(S_1)$ of the singlet fission material. This will allow for energy transfer from the absorbing layer to the singlet fission material where the singlet excitons could be dissociated into triplet excitons. In order to avoid an energetic barrier for the holes the HOMO/valence band energy of this material should be about the same as that of the singlet fission material.

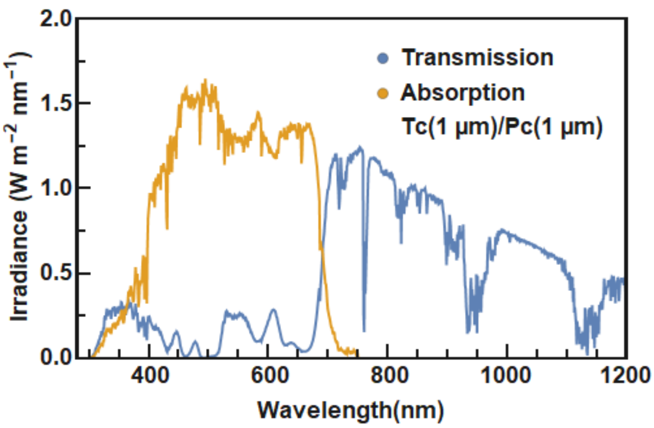

Fig. 2.13: The absorbed (orange) and transmitted (blue) part of the AM1.5G solar spectrum incident on a 1000 nm tetracene layer followed by a 1000 nm pentacene layer.

DCT singlet fission cells show great potential

The simulations show that DCT hybrid silicon/singlet fission devices have the potential to reach efficiencies well beyond the Schockley-Queisser limit even with relatively realistic parameters. The calculated PCE for pentacene and tetracene in a perfectly absorbing device, respectively 28.7% and 29.3% for T = 0.95 and QE = 1.7, show that a 2% absolute gain in efficiency lies within reach for existing materials. Novel materials with more ideal exciton energies, and possible endothermic singlet fission or exciton separation, can reach efficiencies well over 30%. Furthermore, figure 2.11 shows that the singlet fission devices are not only more efficient but also more stable in changing weather conditions.

3 Towards experimental demonstration of direct charge-transfer in hybrid silicon/C_{60}/pentacene solar cells

In this chapter we will focus on a part of the experimental work performed during this internship where we have attempted to make a working DCT singlet fission device. The previous chapter showed that, in theory, DCT can be very successful. However, there are ample of design and fabrication steps that need to be optimised before it will be possible to make a DCT device that beats the base silicon solar cell. For now, the goal is to show a proof-of-principle and provide some evidence of photocurrent originating from singlet fission in DCT solar cells. A very strong indication would be an internal quantum efficiency that rises above 100%.

To this purpose, we prepared multiple batches of DCT solar cells with slightly different architectures and measured their external quantum efficiency. A simple model was developed to decompose EQE measurements of a stack of materials into individual EQE signals. This way, we hope to be able to find evidence of a non-zero IQE for the singlet fission material.

3.1 Device architectures

We will discuss the performance of two different DCT architectures, both based on pentacene. Pentacene was chosen as the singlet fission material because its HOMO level plus triplet exciton energy lies a bit higher than that of tetracene and therefore it should be easier to transfer electrons to the silicon conduction band. Also, pentacene/C_{60} interlayers have been under extensive study and have shown to be very efficient in dissociating triplet excitons into free charge carriers [6, 45].

For the base silicon solar cell we use wafers send to us from the Helmholtz Zentrum in Berlin (HZB), these are n-type doped cristaline silicon wafers (280 μm) with a thin ($\sim 20\mu$m) layer of n+ doped amorphous silicon at the back [26, 20]. Figure 3.1 depicts the layer stacks of the two solar cell approaches presented in this work.

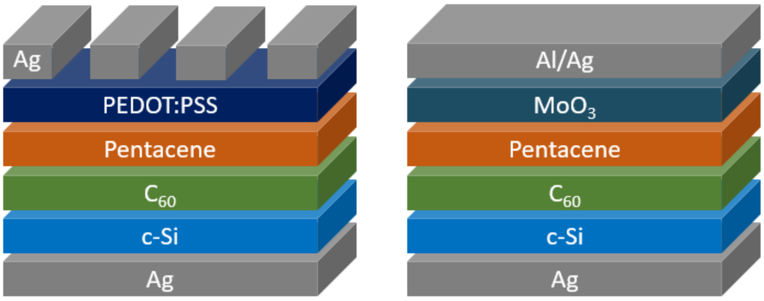

Fig. 3.1: Sketch of the solar cell concepts investigated in this work (layer thicknesses not to scale). Both devices are based on a silicon/C_{60}/pentacene stack but make use of a different hole transporting layer: PEDOT:PSS (left) and MoO_x/Al/Ag (right).

The device concept on the left-hand side incorporates the highly conductive and water soluble polymer PEDOT:PSS (~100 nm) as a hole-selective contact. The pentacene layer has a nominal thickness of 20 nm, the acceptor layer is 0.5 nm thick. The front and back contacts have a thickness of 100 and 200 nm respectively. PEDOT:PSS is commonly used as a hole-selective contact in organic PV singlet fission devices. Liebhaber et al. have also demonstrated its potential in very similar hybrid PEDOT:PSS/silicon and PEDOT:PSS/tetracene/silicon devices [26, 20].

On the right-hand side of figure 3.1 the second architecture is depicted, using a MoO_x (5 nm)/Al (1 nm)/Ag (20 nm) stack as the hole transport layer. This semi-transparent contact (based on the work of Lee et al. [24]) offers the advantage of a very conductive contact that can be made without taking the cell out of the vacuum of the evaporation chamber. The transmission will be about 30% on average over the solar spectrum and the pentacene layer thickness increases from 0 to 40 nm or from 60 to 100 nm on a single sample. The acceptor layer is made of C_{60} (1 nm) and the back contact is identical to the other device: 200 nm of silver.

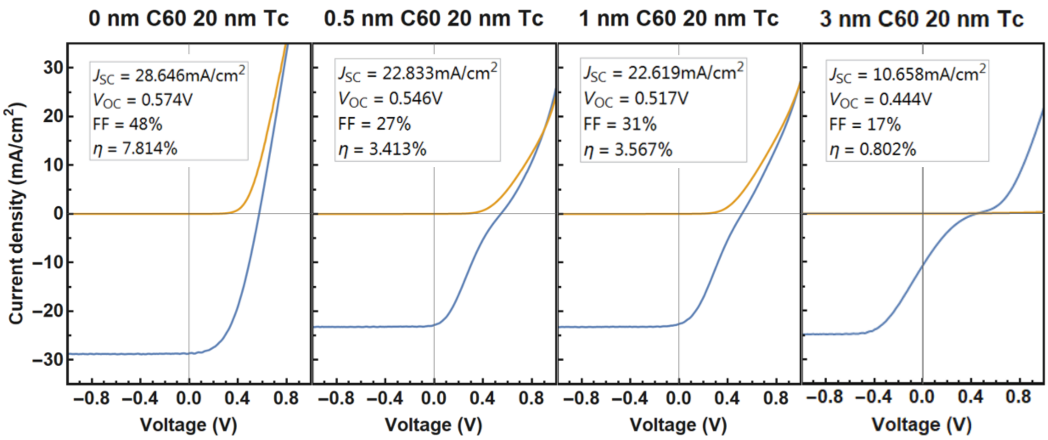

Fig. 3.2: Current-voltage characteristics for tetracene based DCT solar cells (using the PEDOT:PSS hole-transport layer as described in figure 3.1). An increasing layer of C_{60} causes an S-shaped JV-curve which is an indication of an energy barrier in the device. Data presented with permission from M. H. Futscher.

Ideally, the electron acceptor layer would be much thicker as the number of states available greatly enhances the charge separation rate [22]. However, the HOMO-level of C_{60} is very low and would be a huge energetic barrier for the holes originating from the silicon layer. Therefore, it is important that the pentacene layer stays in direct contact with the silicon; this way the holes can be transported unhindered. Based on previous research, we find that its hard to avoid a C_{60} layer to cover the silicon surface when the material is thermally evaporated. In figure 3.2, we show the JV-characteristic for four devices of increasing nominal C_{60} thickness. Apparently, even a 0.5 nm layer induces an S-shape in the current-voltage data indicating an energy barrier in the device. Since practically all the current is generated in the silicon, and there is no S-shape in the no-C_{60} device, the cause of this feature is most likely due to the low HOMO level of C_{60} causing a energy barrier for the holes generated in the silicon. This result is in accordance with literature findings claiming a monolayer-plus-island growth mode of C_{60} on silicon [3], as one monolayer of C_{60} molecules (with a diameter of about 0.7 nm) would already pose a tunnelling barrier large enough to cause the S-shape curves in 3.2. From our data it seems that the S-shape effect does not get worse for C_{60} layers up to 1 nm, which is why we do not make use of thicker fullerene layers in the presented device architectures.

Details about the fabrication processes are given in the following section.

3.2 Methods

3.2.1 Device fabrication

Cutting the wafer

The wafers received from the HZB are cut on site using a high speed saw. We first spincoat the wafers with S1813 (Microposit G2). The resist is poured on the wafer, until it is covered, while it is spinning at a moderate speed. Afterwards the wafers are spincoated for 45 seconds at 4000 rpm and baked on a 110°C hotplate for 3 minutes. The process is repeated for the other side of the wafer and gives a 1.5 μm layer that protects the silicon during the sawing process. After spincoating the wafer is glued on a plastic foil. The wafers are diced in squares of 15x15 mm with a partial cut of 100 μm deep, from the back of the cell, 2.5 mm from the edge of each 15x15 mm square. In the final stages of the sample preparation these 2.5 mm strips can be clipped off to give a 10x10 mm cell with very clean edges.

Cleaning procedure

The silicon slides are removed from the plastic foil and given an initial rinse of aceton to get rid of the S1813 resist layer. The slides are then cleaned with a detergent (Omniclean RBS 25), deionised water and a soft toothbrush, and rinsed with deionised water to get rid of the soap. Afterwards they are rinsed and subsequently submerged in aceton to be sonificated for approximately 15 minutes. The sonification procedure is repeated twice with aceton and twice with isopropanol. The slides are then taken out of the isopropanol and are dried with a nitrogen gun.

HF procedure
To remove the native oxide on the silicon slides the samples are submerged in a 2% HF solution for exactly 3 minutes. They are then dipped quickly into a deionised water bath for a couple of seconds and dried with a nitrogen gun. After HF-etching the slides are transported to the oxygen-free environment of the glovebox as quickly as possible, usually within 10 minutes.

Thermal evaporation procedure
The organic layers are deposited using thermal evaporation in a modified Angstrom Engineering Amod vacuum system. The organics are sublimated from Radak-II silica crucibles of which the temperature can be monitored during deposition. Organics are only deposited at pressures below 10^{-6} Torr. Both the C_{60} (99.9% purity) and pentacene (99.995% purity) layers are deposited at a rate of 0.5 Å/s while the substrate rotation is set to 50%.

Metals are evaporated at pressures from $10^{-}5$ Torr, without substrate rotation starting at a rate 0.5 Å/s. The rate is increased to 1.0 Å/s after a thickness of 10 nm.

Spincoating PEDOT:PSS hole-selective layer
The PEDOT:PSS solution (Clevios Solar, F High Conductivity) is stored in the refrigerator in an airtight container and is sonificated for approximately 15 minutes before spincoating. Following the same recipe as the HZB, 170 μL of PEDOT:PSS solution is applied in such a way that it covers the full surface of the 15x15 mm silicon slide. The cells are then spincoated at 2000 rpm with 666 rpm/second acceleration for 20 seconds. Afterwards the films are annealed for approximately 60 minutes on a hot-plate of 60 °C in the glovebox.

Finishing the solar cell
Finally, the 2.5 mm wide edges are clipped off using two tweezers, without touching the middle square of silicon slides. This step makes sure that there is no left-over material from evaporation or spincoating on the sides of the solar cell, which could create a short and reduce the device performance.

The cells are then glued to a clean copper plate of 15x15 mm with two-phase silver epoxy (Chemtronics CW2400). The completed cells are stored in the glovebox overnight to make sure the epoxy is completely hardened before measurement.

3.2.2 Analytical methods

JV measurements

The current-voltage characteristics presented in this report are measured using an Agilent B2902A source-measure unit. The dark curve is measured under a piece of aluminium foil and the light-curve under a solar simulator manufactured by Newport (Model: Oriel instruments Sol 2A). The lamp was turned on at least an hour before measurement and the intensity was tuned to 1 sun with the help of a silicon reference detector. Great care was taken to place the sample at the same location as the reference cell.

Quantum efficiency measurements

The quantum efficiency was measured in a Newport Oriel QuantX-300 measurement solution [18]. The setup (figure 3.3) consists of a Xenon lamp, the light passes through a chopper wheel, a filter and a monochromator where a certain wavelength is selected. This monochromatic light then gets reflected from a beam-splitter before it hits the sample. The copper plate and front contact of the sample are connected with metal probes to measure the generated photocurrent. Due to ambient lighting, this signal is often noisy, and needs to be send to a lock-in amplifier where the modulated photocurrent gets extracted. A voltage bias of up to (-)10 V can be applied over the sample. The light that gets reflected from the sample can pass through the beam-splitter to be detected by a reflectance monitor. The setup cannot account for diffusely reflected light.

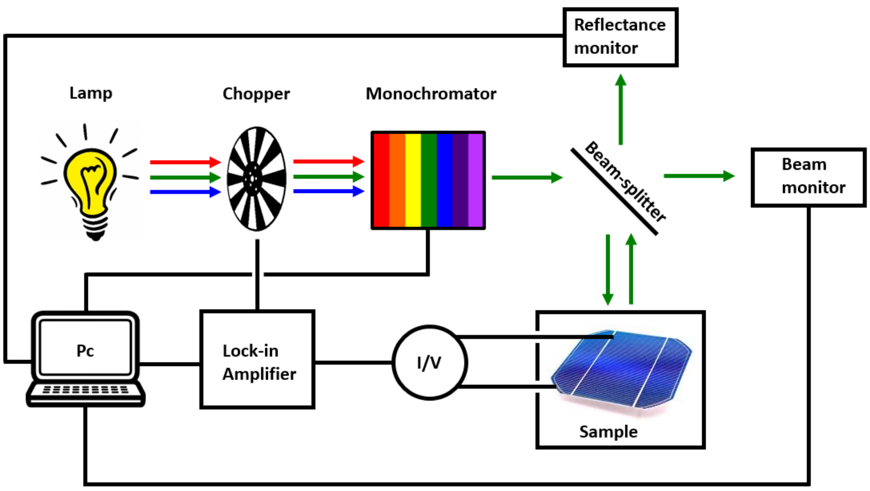

Fig. 3.3: Schematic setup of the QuantX-300 EQE measurement system.

Before operation the reflectance and beam monitor first need to be calibrated (after the lamp has been turned on for at least 30 minutes to warm up and stabilise). To calibrate the light intensity on the sample the beam monitor is calibrated with a second monitor at the sample position by performing a scan over the whole wavelength range. To calibrate the reflectance monitor we place a mirror of high and low reflectivity at the sample stage, aim the reflected light back through the reflectance monitor, and perform another scan over the wavelength range. Afterwards, a reference silicon solar cell is measured to check the calibration.

The current-voltage characteristics are measured before starting the EQE measurements. This way we can decide beforehand if a voltage bias will be necessary to extract an appreciable current from the cells. All devices of one batch are measured at a bias where even the worst cell can be measured. Before starting a EQE measurement the sample stage is ajusted to maximise the signal from the reflectance monitor to make sure the reflected light is correctly aligned.

UV/VIS spectroscopy
Absorption measurements were taken using a PerkinElmer 750 Lambda UV-VIS system. The system was turned on at least half an hour before measurement to stabilise the lamp. The light was always aligned before measuring and a 0% baseline measurement was carried out on a cleaned substrate (identical to the sample substrate).

AFM
Atomic force microscopy measurements were carried out in air using a Bruker Dimension Icon with ScanAsyst.

3.2.3 EQE model and fitting procedure

Here, we will construct a simple model to describe the EQE data of a solar cell made from a stack of materials. The external quantum efficiency is defined as the ratio of the number of of charge carriers collected from a solar cell to the number of incident photons of a given wavelength. In the hybrid devices, however, there are multiple layers that can contribute to the photocurrent, not only the silicon wafer but also the pentacene and other (organic) layers absorb light and deliver charge carriers. Therefore, an EQE spectrum can be treated as the sum of all individual EQE spectra of the contributing layers. If we furthermore decompose the EQE spectra in the internal quantum efficiency (the number of carriers per absorbed photon) times the absorption spectrum of the active layer in the solar cell and approximate the internal quantum efficiency of every contributing layer as a constant over all wavelengths we end up with the following formula:

$$EQE(\lambda) = \sum_i IQE_i(\lambda) \cdot Abs_i(\lambda) \approx \sum_i constant_i \cdot Abs_i(\lambda) \tag{3.1}$$

Where $EQE(\lambda)$ gives the total EQE of the solar cell at a certain wavelength, $IQE_i(\lambda)$ and $Abs_i(\lambda)$ give, respectively, the internal quantum efficiency and the absorption of each individual active layer at that specific wavelength and $constant_i$ gives the IQE of the layer under the assumption that its value does not change over the spectrum.

Determining the absorption term in equation 3.1 can be challenging because the absorption spectrum of each layer cannot be measured independently. Due to interference effects the optical density of the stack is not simply the sum of the optical density of each individual layer. Therefore, it generally takes optical modelling to relate the (experimentally measurable) total absorption of a stack of materials to the absorption of each individual layer. To this purpose, we use the code based on the TransferMatrix model developed in the McGehee group at Stanford University [1]. This method calculates the interference of coherent reflected and transmitted waves at each interface as well as the absorption of each layer in the solar cell. The model requires the wavelength dependent complex index of refraction of all the materials in the stack. The real part n determines the speed of light of a given energy inside the material and is important for calculating the interference (constructive an destructive) in the stack and therefore the field intensity profile in the cell. The imaginary part k, often called the extinction coefficient, determines the absorption of the light.

Using a library of all the experimentally measured complex refraction indices of the materials used in this research the absorption terms of equation 3.1 can be calculated and the formula can be fitted to the measured EQE spectrum. The thickness and the (wavelength independent) IQE of each layer in the stack are used as fitting parameters. Only the layers that are thought to contribute to the photocurrent are given a nonzero IQE.

During the EQE-analysis, first, the thicknesses of all the layers is varied to best fit the calculated reflection to the reflection measured in the EQE-setup, allowing for a 50% deviation from the nominal thickness indicated by the evaporator thickness monitor. Then, the IQE of each layer is varied to best fit the measured EQE spectrum.

Please note that the TransferMatrix model assumes all layers in the stack to be flat. While this is a relatively fair assumption for thermally evaporated metal films and the spincoated films of PEDOT:PSS (as long as the evaporation/spincoating is performed on a flat surface), for the organic layers made by thermal evaporation this is generally not the case. The overall optical properties, especially influenced by the internal reflections, can depend strongly on the morphology of the films. Furthermore, processing conditions such as temperature, age and layer thickness might change the morphology of the films [2] and thus the optical constants.

3.3 Results

3.3.1 PEDOT:PSS device performance

In the following section PEDOT:PSS/Pentacene/C_{60}/silicon hybrid devices, as described in section 3.1, are evaluated by means of their current-voltage characteristics and EQE spectra. Additionally, EQE measurements are analysed by fitting the experimental data with the extended TransferMatrix model described in section 3.2.3. We will discuss the current-voltage and EQE measurements of the highest efficiency device of the batch.

In figure 3.4 the current-voltage characteristic of the best performing, PCE = 3.46%, device is shown. The slight S-shape in the JV-curve might be the result of an energy barrier for one of the charges.

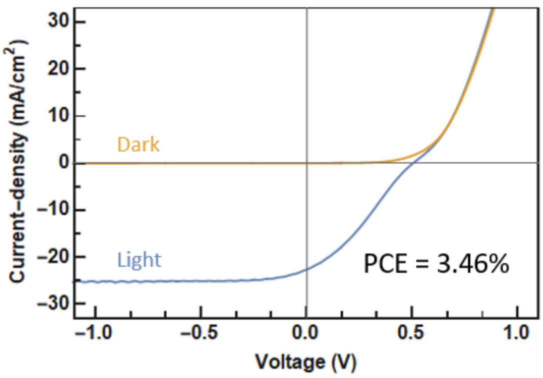

Fig. 3.4: The current-voltage characteristic of the best performing PEDOT:PSS device.

In figure 3.5 the EQE spectrum of the best performing device is shown. The spectrum shows a relatively high EQE plateau before the EQE drops to zero at a wavelength around 1100 nm, features characteristic for a silicon solar cell, but there is a significant decrease in EQE between 500 and 700 nm. These features are the effect of absorption in pentacene. Unfortunately, the fact that the EQE drops in this region already shows that the IQE of the pentacene layer cannot be higher than the silicon IQE and thus, the possible triplet origin of the pentacene photocurrent cannot be proven directly.

Figure 3.5 also shows the fit to the EQE spectrum. To obtain this fit we followed the procedures as discussed in the previous section. The reflectance measurement could be fitted with reasonable accuracy with the TransferMatrix model using layer thicknesses close to the expected values. PEDOT:PSS layer thickness was set to 115 nm where we expected a roughly 100 nm layer from the recipe. The pentacene layer thickness was set to the nominal thickness as indicated by the evaporation

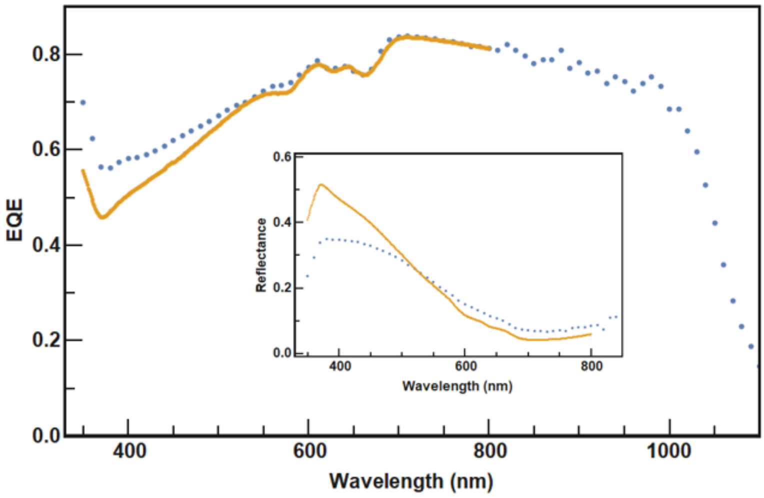

Fig. 3.5: The EQE spectrum of the best performing PEDOT:PSS device. The reflectance as measured in the EQE setup is shown in the inset. The blue dots give the measured value, the solid orange lines give the fit to both the EQE and reflectance using the fitting parameters displayed in table 3.1.

system. The fitted curve describes the general behaviour of the reflectance and stays fairly close (within 3% absolute) to the measured reflectance in the pentacene absorption wavelength range (500 - 700 nm) which is the region we are interested in. The measured reflectance starts to deviate significantly from the fitted value at wavelengths below 500 nm.

A reason for the deviation of the fitted reflectance from the measured data could be the optical anisotropic behaviour of PEDOT:PSS. Liebhaber et al. [26] find that the material is birefringent and shows ordinary and extraordinary components in the extiction coefficient, in the parallel and perpendicular axis to the surface normal, when spincoated on a flat substrate. Since the surface of the evaporated pentacene films are quite rough, both components have to be taken into account which can cause significant changes in the n- and k-values. Thus, the literature values used to fit the data can be quite different from the optical constants in the PEDOT:PSS films of the devices. The fact that the optical constants of pentacene in the TransferMatrix library are only known from 450 nm (and are set to 0 for lower wavelengths) can also partially explain the mismatch between the measured reflectance and the fitted curve.

Tab. 3.1: Fitting parameters for the EQE measurement of the best PEDOT:PSS contact device. The C_{60} IQE has been set to zero since the material hardly absorbs any light and does not influence the fit.

	PEDOT:PSS	Pentacene	C_{60}	Silicon
Thickness	115 nm	20 nm	0.5	∞
Fitted IQE	0.45	0.25	0	1.00

Table 3.1 gives the parameters used to generate the fitted EQE-curve. The fit to the EQE spectrum in figure 3.5 is in excellent agreement with the data in the pentacene region and worsens towards lower wavelengths as expected from the reflectance-fit. Estimating the error on the presented IQE parameters is difficult since both the reflectance fit and the EQE fit will result in an error on the given IQE values. The reflectance fit gives an error on the fitted layer thicknesses and does not perfectly describe the measured reflectance. The errors on the layer thicknesses are not very large as the evaporated pentacene thickness is well-calibrated and the assumption that silicon is thick enough to absorb all the light is very reasonable, so, in principle, only the PEDOT:PSS layer thickness carries a significant error. However, the issues regarding the optical parameters of the materials involved causes extra uncertainty. Assuming the reflectance fitting procedure does not bring any error, we estimate the error on the IQE-values to be 2% for silicon and 5% for PEDOT:PSS and pentacene. As deviations beyond these margins lead to a significantly worse fit. In any case, the EQE data is not consistent with a pentacene IQE of 0% for any set of parameters, as lowering the pentacene thickness will lead to significant issues with the reflectance fit. Furthermore, the EQE analysis on the other cells of the batch consistently give similar IQE values. Thus, the pentacene IQE might be small, but it seems that the material does contribute to the photocurrent.

The fitted IQE for the pentacene layer of 0.25, on a scale of 0 to 2, indicates that the pentacene contribution to the photocurrent is quite low. Nevertheless, the fact that we find a pentacene contribution already shows that the device architecture works. We are able to generate singlet excitons in the pentacene layer and some of these excitons, whether it may be triplets or singlets, are separated into free charges. These free charges can be collected at the top- and bottom contacts which indicates that the electrons are able to transfer to the silicon.

The best fit was acquired for a silicon IQE of 1.00 which shows that the quantum efficiency of the silicon cell is hardly affected by the additional organic layers. Apparently, the holes generated in the silicon have a near unity probability of being collected at the front contact which shows excellent hole-mobility in pentacene and indicates that there are no large energetic barriers. For a good fit PEDOT:PSS needs an IQE value of 0.45, indicating that it does contribute to the total photocurrent of the device. Presumably, the excitons generated in the PEDOT:PSS layer are transferred to the pentacene (the HOMO-LUMO offset of PEDOT:PSS is slightly larger than that of pentacene) where the exciton(s) can be separated at the C_{60} interface or the pentacene acts as an electron acceptor and the exciton is separated at the PEDOT:PSS/pentacene interface.

3.3.2 MoO_x/Al/Ag device performance

Here the hybrid singlet fission devices using a MoO_x/Al/Ag hole-selective contact, as described in section 3.1, will be discussed by means of their current-voltage characteristics and EQE spectra. The EQE measurements are fitted with the model described in section 3.2.3 to gain additional information on the pentacene IQE.

In this batch the thickness of the pentacene layer has been varied from 0 nm to a 100 nm. In figure 3.6 the current-voltage characteristic is shown for the 0 - 40 nm pentacene device (left) and the 60 - 100 nm pentacene device (right). The generated photocurrent is fairly low because the MoO_x/Al/Ag top contact is very reflective; on average only 30% of the incident light is transmitted to the pentacene layer [25]. Also, the 0 to 40 nm pentacene device performs better compared to the thicker pentacene layer solar cell with a PCE of respectively 1.03% and 0.03%. It is hard to pinpoint the exact mechanism behind the strong S-shape curve of the thicker layered device but most likely the increased thickness causes problems for the hole transport trough the pentacene layer. Charges travelling trough organic layers have to hop between the molecular orbitals and because the orbital energies can slightly shift from molecule to molecule (as a result of minor changes in its orientation) the holes might need a certain voltage to drive them over these small energy barriers, which would explain the S-shaped curve.

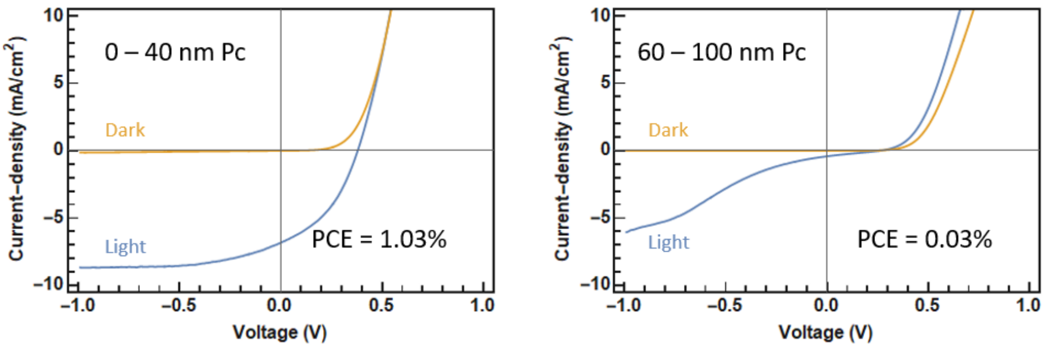

Fig. 3.6: The current-voltage characteristic of the Ag/Al/MoO_3 devices with 0 to 40 nm pentacene layer (left) and 60 to 100 nm pentacene layer (right).

The EQE measurements shown in figure 3.7 have been performed under a voltage bias of -1.0 V. The significant reflection from the metalised front surface has altered the the typical silicon EQE-shape; the EQE is high at lower wavelengths and gradually decreases until, at the silicon bandgap, the signal drops to zero. Between 500 nm and 700 nm the absorption profile of pentacene is clearly visible and, as expected, we can see a gradual increase of the depth of this dip for thicker layers of pentacene. Again, the dip in EQE in the absorption range of pentacene means that the IQE of pentacene is lower than that of the silicon layer in these devices and, thus, there is no direct evidence of singlet fission contributing to the photocurrent.

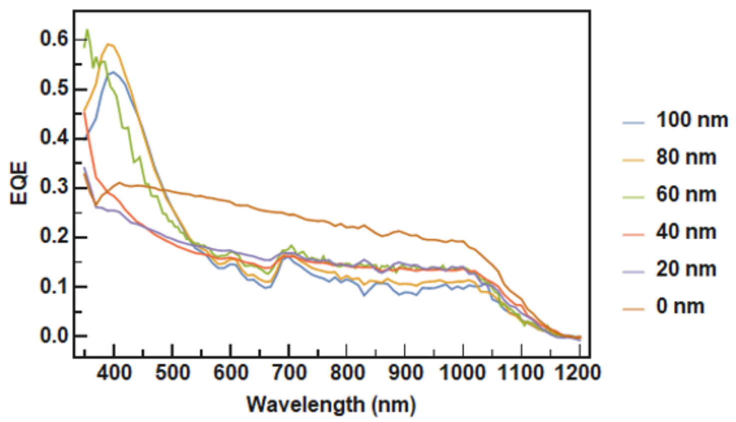

Fig. 3.7: The EQE spectra of the Ag/Al/MoO_3 devices with increasing pentacene layer thickness. All spectra were measured at a -1 V bias.

To get the individual IQE values of the materials contributing to the photocurrent the EQE spectra are fitted following the procedure described in section 3.2.3. Unfortunately, it is not possible to get a reasonable fit to the reflectance data using the n- and k-values for the materials in our library. This implies that the n- and k-values from literature do not match the values of the materials used, the scattering processes in the layer stack have a significant effect on the reflectivity, or the reflectivity measurement is faulted. A major concern is the fact that we were not able to fit the EQE spectrum for the device without pentacene, the shape of the silicon absorption in the material stack does not match the general shape of the EQE measurement. Although, for most samples, a reasonable fit on the EQE spectrum can be obtained by tuning the layer thicknesses and IQE values, the results have to be treated with great caution. Especially because the fit on the reflectance is off where pentacene is absorbing (500-700 nm).

In figure 3.8 the best fit on the 60 nm pentacene sample is shown. The layer thicknesses used in the TransferMatrix model together with the fitted IQEs are listed in table 3.2. The thickness parameters are fairly close to the nominal thickness as indicated by the evaporator software except for the molybdenum trioxide layer which was thought to be only 5 nm. The evaporated thickness of this material should be measured to test the validity of this parameter in the fitting model. To account for the EQE-peak just below 400 nm the MoO_x IQE-value has been set to 1, this is very high and probably not realistic. Because the absorption profile of silicon in this material stack does not match the general EQE shape (at lower wavelengths we seem to need higher silicon IQE), the fitted silicon IQE had to be set to 0.6 to match the EQE signal in the pentacene absorption region and probably is not very accurate.

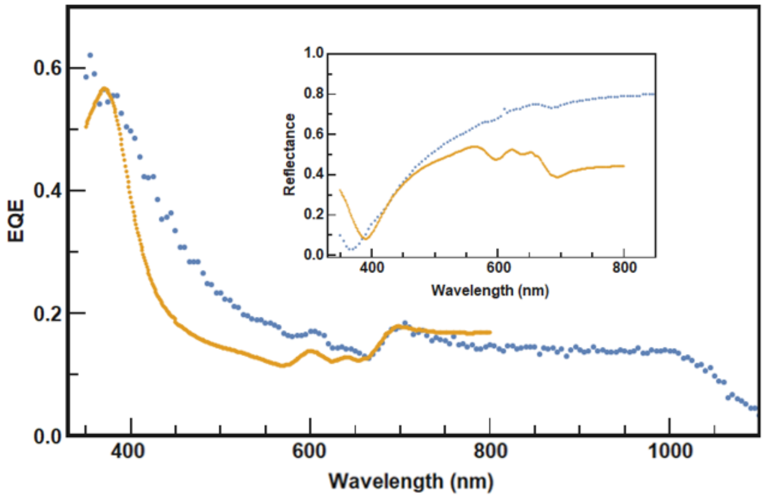

Fig. 3.8: The EQE spectrum of the 60 nm pentacene Ag/Al/MoO_3 device. The reflectance as measured in the EQE setup is shown in the inset. The blue dots give the measured value, the solid orange lines give the fit to both the EQE and reflectance using the fitting parameters displayed in table 3.1.

The fits on the other samples, performed with the same thickness parameters except for the pentacene thickness which was always set on the evaporated thickness, are of similar quality. To fit the other EQE spectra only the pentacene and silicon IQE was varied. We were unable to fit the EQE spectra of the 0 nm and 20 nm pentacene measurements.

Tab. 3.2: Fitting parameters for the EQE measurement of the 60 nm pentacene MoO_x contact device. The C_{60} IQE has been set to zero since the material hardly absorbs any light and does not influence the fit. Obviously, metals cannot contribute to the photocurrent so their IQE has been set to zero as well.

	Ag	Al	MoO_x	Pentacene	C60	Silicon
Thickness	16 nm	1 nm	12 nm	60 nm	1 nm	∞
Fitted IQE	-	-	1.0	0.2	-	0.6

The pentacene IQE varied from 0.15 in the 100 nm pentacene sample to 0.35 in the 40 nm pentacene sample, giving the impression that the charge separation gets more efficient for thinner layers of pentacene. This would make sense, since the the triplet exciton diffusion length is only 40 nm [39]. The triplets have to diffuse to the donor/acceptor interface before the charges can be dissociated, therefore thicker layers will give more time for recombination processes.

3.4 Discussion

In both architectures we have been able to provide evidence of a pentacene contribution to the photocurrent of similar magnitude (although the results from the

MoO_x/Al/Ag devices should be treated with caution), with an IQE of roughly 0.20 to 0.25 on a scale of 0 to 2. This is too low to show, from the EQE alone, that the photocurrent originates from singlet fission but it does show that there is some exciton generation, that the excitons can be successfully separated and that the resulting electrons and holes are able to find their respective contacts.

The low pentacene IQE can, partially, be explained by the thin C_{60} layers. Usually, singlet fission cells are made using thick pentacene/fullerene bilayers as the availability of states is thought to be the most important indicator for efficient charge separation [22]. Furthermore, using a planar heterojunction requires the triplet excitons to diffuse to the C_{60} interface which gives more time for recombination processes to occur. To increase the pentacene contribution in future devices bulk heterojunctions might be unavoidable, however, in hybrid DCT devices we want to avoid covering the entire silicon surface with fullerenes as this will cause a significant energetic barrier for the holes originating from the silicon cell, see figure 2.2 and 3.2.

The main reason for low pentacene IQE is thought to be an energy barrier for the electrons resulting from exciton dissociation in the C_{60} layer. Chen et al. find a 30 meV energetic barrier between the LUMO-level of C_{60} and the valence band of n-doped crystalline silicon [4]. Since the LUMO-level of C_{60} can be severely altered by the presence of other materials this energy barrier might be different in the devices discussed in this report. However, in case an energetic barrier is present in our devices this will definitely lower the transfer efficiency of electrons across the C_{60}/silicon interface and therefore the IQE of the pentacene layer. It might be possible to lower the possible energy barrier by chemical modification of the silicon surface using interfacial doping or self-assembled monolayers [17].

The PEDOT:PSS cells show that with a good hole-selective contact the silicon IQE is hardly affected. Thus, hole transfer trough a 20 nm pentacene film and the silicon/pentacene and pentacene/PEDOT:PSS interfaces is almost lossless. To provide evidence of photocurrent originating from singlet fission without the need for pentacene IQE above 1, one can measure the magnetic field dependence of the photocurrent [27, 36]. As a magnetic field would partially suppress the formation of triplets it will also lower the photocurrent resulting from singlet fission. The dependence of the change in photocurrent for increasing magnetic field strength gives a characteristic profile commonly known as the *Merrifield curve*. Depending on the sign of this curve (growing or decreasing photocurrent for increasing field strength) this would give a strong indication for either singlets or triplets contributing to the photocurrent of the devices.

For future investigations using the EQE model proposed in this report we have a few recommendations:

- Simpler device architectures are preferable. More material layers make it increasingly difficult to accurately fit the reflection and EQE data and, arguably, increases the errors in the fits.

- Organic films are often quite rough which will cause scattering effects, this is not accounted for in the TransferMatrix model. It might be worth considering to switch to a model that can account for a rough film morphology, for example the MATLAB software package *GenPro4*, developed at the Delft University of Technology [31].

- To improve the fit to the EQE data, especially over a larger wavelength range, it might be more accurate to change the constant IQE value for every material layer to a constant times the, normalised, absorption spectrum of that material.

- The PEDOT:PSS hole-selective layer, although very effective, might cause problems due to its the birefringent properties. It can be worthwhile to investigate the feasibility of other hole-selective contacts such as MoO_x/ITO (Indium Tin Oxide).

4 Conclusion & outlook

4.1 Conclusion

Today silicon photovoltaic technology is dominating the global market with a total market share of over 95% and efficiencies reaching as high as 26.7%. However, conventional silicon cells have a hard efficiency limit of 29.4% (Auger limited) and, therefore, the ever increasing efficiency of state-of-the-art silicon devices will soon come to a halt if we do not change our strategy. Singlet fission might be an effective approach to fight thermalisation losses, the most substantial loss mechanism in silicon based solar cells, accounting for 33% of the solar irradiation. Successful implementation of singlet fission could increase the Schockley-Queisser limit from 33% to 42% (E_g = 1.1 eV, not including Auger recombination).

To this purpose we propose a device in which the triplet excitons in the singlet fission material are separated using a fullerene electron acceptor. This has been shown to work very efficiently on sub-100 fs timescales in pentacene/C_{60} bilayer systems. The resulting electrons will have to transfer across the fullerene/silicon interface to be collected at electron contact at the back of a silicon wafer and the holes originating from both the silicon cell and the singlet fission layer have to be collected at the top of the cell using a hole-selective contact.

The performance of the proposed charge-transfer device has been simulated under both standard test conditions and real weather data. These simulations have shown that the proposed architecture has the potential to reach well beyond the Auger-limited Schockley-Queisser limit. Incorporating pentacene or tetracene as the singlet fission material, power conversion efficiencies of respectively 28.7% and 29.3% can be reached (assuming perfect absorption above $E(S_1)$), a singlet fission quantum efficiency of 1.7 and 90% light transmission to the silicon base cell), showing that a 2% absolute improvement on the current record silicon power conversion efficiency is possible even for existing singlet fission materials. Optimised, novel, materials could help to increase the power conversion efficiency to values well over 30%. In contrast to series tandem solutions the direct charge-transfer devices do not suffer from major losses in changing weather conditions. Moreover, due to the reduction in thermalisation losses, the singlet fission cell efficiency is more stable, under spectral illumination of higher average photon energy when compared to silicon solar cells.

However, there are many challenges to overcome before these devices can become reality. First of all, we assumed total absorption of all light above E(S_1) which, for present materials, is not possible with the singlet fission material alone as the absorption is often low and thick layers will induce losses in efficiency. Clever solutions are needed to enhance the absorption in the singlet fission layer and/or absorb the light in a different material and, subsequently, donate the singlet excitons to the singlet fission material. Second, to reach power conversion efficiencies over 30% novel, efficient, singlet fission materials with optimised singlet and triplet energies are essential.

In chapter 3 of this report we discussed the experimental work on two direct charge-transfer architectures, both based on pentacene, that have been analysed using their current-voltage characteristics and external quantum efficiency. We have developed a simple model to decompose the EQE spectrum of a stack of materials into internal quantum efficiencies of the individual layers. The pentacene in both cell designs shows an internal quantum efficiency of about 20 to 25%, and thus, does not offer any evidence of singlet fission. However, it does show that the direct charge-transfer principle can work. Apparently, there is some photocurrent originating from the pentacene so part of the excitons, triplets or singlets, is successfully separated into free charges and some of the electrons are able to transfer to the silicon cell. Furthermore, the internal quantum efficiency of the underlying silicon cell is hardly affected by the organics in case of a good hole-selective contact (the fitted internal quantum efficiency of silicon in the PEDOT:PSS device was estimated at 1.0) which shows that the holes generated in the silicon cell can transfer to the top contact almost unhindered.

4.2 Outlook

The model described in chapter 2 can easily be expanded to simulate the performance of hybrid singlet fission devices utilising other energy transfer mechanisms, such as Förster resonance energy transfer and Dexter enery transfer approaches. Finally, it can be worthwhile to simulate the performance of direct charge-transfer devices when the silicon layer is changed to a different material, such as $CuIn_xGa_{1-x}Se_2$, CdTe or perovskite.

To find evidence of a singlet-fission-originated photocurrent the magnetic field dependence of the proposed cells can be measured. As a magnetic field would partially suppress the formation of triplets it will also lower the photocurrent resulting from singlet fission. The dependence of the change in photocurrent for increasing magnetic field strength gives a characteristic curve and can provide information on the triplet or singlet origin of the photocurrent. This Merrifield curve could give a strong indication for singlet fission contributing to the photocurrent of the devices.

According to the model presented in this report a hybrid silicon/singlet fission device that breaks the Schockley-Queiser limit lies within reach. To reach this goal, the singlet fission community should focus on making new materials with desirable exciton energies and increasing absorbance in the singlet fission layer. The experimental results show that there is still a lot of work to be done on device engineering and the understanding of the energy transfer processes at the material interfaces. Even so, the singlet fission field has only recently started to work on hybrid organic/inorganic singlet fission devices. Nonetheless, considerable progress has been made over the last few years and with combined effort from engineers, material scientist and, importantly, synthetic chemists this promises to be an exciting time.

Bibliography

[1] G. F. Burkhard, E. T. Hoke, and M. D. McGehee. „Accounting for Interference, Scattering, and Electrode Absorption to Make Accurate Internal Quantum Efficiency Measurements in Organic and Other Thin Solar Cells". In: *Advanced Materials* 22.30 (2010), pp. 3293–3297. eprint: `https://onlinelibrary.wiley.com/doi/pdf/10.1002/adma.201000883` (cit. on pp. 22, 31).

[2] M. Campoy-Quiles, T. A. M. Ferenczi, T. Agostinelli, et al. „Morphology evolution via self-organization and lateral and vertical diffusion in polymer:fullerene solar cell blends." In: *Nature materials* 7.2 (2008), pp. 158–64 (cit. on p. 31).

[3] D. Chen and D. Sarid. „Growth of C60 films on silicon surfaces". In: *Surface Science* 318.1 (1994), pp. 74–82. eprint: `http://www.sciencedirect.com/science/article/pii/0039602894903425` (cit. on p. 27).

[4] K. M. Chen, Y. Q. Jia, S. X. Jin, et al. „Heterojunctions of solid C 60 and crystalline silicon: rectifying properties and energy-band models". In: *Journal of Physics: Condensed Matter* 7.14 (1995), p. L201. eprint: `http://stacks.iop.org/0953-8984/7/i=14/a=004` (cit. on p. 38).

[5] C. Chu, Y. Shao, V. Shrotriya, and Y. Yang. „Efficient photovoltaic energy conversion in tetracene-C60 based heterojunctions". In: *Applied Physics Letters* 86.24 (2005), p. 243506. eprint: `https://doi.org/10.1063/1.1946184` (cit. on p. 10).

[6] D. N. Congreve, J. Lee, N. J. Thompson, et al. „External Quantum Efficiency Above 100% in a Singlet-Exciton-Fission–Based Organic Photovoltaic Cell". In: *Science* 340.6130 (2013), pp. 334–337. eprint: `http://science.sciencemag.org/content/340/6130/334.full.pdf` (cit. on pp. 9, 10, 25).

[7] B. Daiber. „Research update - singlet fission solar cells". LMPV quarterly meeting. 2018 (cit. on p. 9).

[8] D. L. Dexter. „A Theory of Sensitized Luminescence in Solids". In: *The Journal of Chemical Physics* 21.5 (1953), pp. 836–850. eprint: `https://doi.org/10.1063/1.1699044` (cit. on p. 9).

[9] J. Dziewior and W. Schmid. „Auger coefficients for highly doped and highly excited silicon". In: *Applied Physics Letters* 31.5 (1977), pp. 346–348. eprint: `https://doi.org/10.1063/1.89694` (cit. on p. 11).

[10] T. Förster. „Energiewanderung und Fluoreszenz". In: 33 (1946), pp. 166–175 (cit. on p. 9).

[11] R. H. Friend, M. Phillips, A. Rao, et al. „Excitons and charges at organic semiconductor heterojunctions“. In: *Faraday Discussions* 155 (2012), p. 339. eprint: http://adsabs.harvard.edu/abs/2012FaDi..155..339F (cit. on p. 9).

[12] M. H. Futscher and B. Ehrler. „Efficiency Limit of Perovskite/Si Tandem Solar Cells“. In: *ACS Energy Letters* 1.4 (2016), pp. 863–868. eprint: https://doi.org/10.1021/acsenergylett.6b00405 (cit. on pp. 3, 11, 12).

[13] M. H. Futscher and B. Ehrler. „Modeling the Performance Limitations and Prospects of Perovskite/Si Tandem Solar Cells under Realistic Operating Conditions“. In: *ACS Energy Letters* 2.9 (2017), pp. 2089–2095. eprint: https://doi.org/10.1021/acsenergylett.7b00596 (cit. on pp. 3, 11).

[14] M. H. Futscher, A. Rao, and B. Ehrler. „The Potential of Singlet Fission Photon Multipliers as an Alternative to Silicon-based Tandem Solar Cells“. In: *ArXiv e-print* (2018). arXiv: 1807.09978 (cit. on pp. 2, 3, 9, 11, 19–21).

[15] M. A. Green. „Commercial progress and challenges for photovoltaics“. In: *Nature Energy* 1.1 (2016), p. 15015 (cit. on p. 8).

[16] M. A. Green, Y. Hishikawa, E. D. Dunlop, et al. „Solar cell efficiency tables (version 52)“. In: *Progress in Photovoltaics: Research and Applications* 26.7 (2018), pp. 427–436. eprint: https://onlinelibrary.wiley.com/doi/pdf/10.1002/pip.3040 (cit. on pp. 1, 9, 14).

[17] T. He, H. Ding, N. Peor, et al. „Silicon/Molecule Interfacial Electronic Modifications“. In: *Journal of the American Chemical Society* 130.5 (2008). PMID: 18181625, pp. 1699–1710. eprint: https://doi.org/10.1021/ja0768789 (cit. on p. 38).

[18] Oriel instruments. *QUANTX-300 Quantum Efficiency Measurement Solution*. Newport. 31950 East Frontage Road, Bozeman, Montana, U.S.A, 2018. eprint: www.newport.com/b/oriel-instruments (cit. on p. 29).

[19] *International Energy Agency Technology Roadmap Solar Photovoltaic Energy*. 2014. eprint: https://www.iea.org/publications/freepublications/publication/TechnologyRoadmapSolarPhotovoltaicEnergy_2014edition.pdf (cit. on p. 1).

[20] S. Jäckle, M. Liebhaber, C. Gersmann, et al. „Potential of PEDOT:PSS as a hole selective front contact for silicon heterojunction solar cells“. In: *Scientific Reports* 1.7 (2017), pp. 2045–2322. eprint: https://doi.org/10.1038/s41598-017-01946-3 (cit. on pp. 25, 26).

[21] A. C. Jakowetz, M. L. Böhm, J. Zhang, et al. „What Controls the Rate of Ultrafast Charge Transfer and Charge Separation Efficiency in Organic Photovoltaic Blends“. In: *Journal of the American Chemical Society* 138.36 (2016). PMID: 27538341, pp. 11672–11679. eprint: http://dx.doi.org/10.1021/jacs.6b05131 (cit. on p. 10).

[22] A. C. Jakowetz, M. L. Böhm, J. Zhang, et al. „What Controls the Rate of Ultrafast Charge Transfer and Charge Separation Efficiency in Organic Photovoltaic Blends“. In: *Journal of the American Chemical Society* 138.36 (2016). PMID: 27538341, pp. 11672–11679. eprint: https://doi.org/10.1021/jacs.6b05131 (cit. on pp. 27, 38).

[23] R. C. Johnson and R. E. Merrifield. „Effects of Magnetic Fields on the Mutual Annihilation of Triplet Excitons in Anthracene Crystals“. In: *Phys. Rev. B* 1 (2 Jan. 1970), pp. 896–902. eprint: https://link.aps.org/doi/10.1103/PhysRevB.1.896 (cit. on p. 8).

[24] J. M. Lee, M. H. Futscher, L. M. Pazos-Outón, and B. Ehrler. „Highly transparent singlet fission solar cell with multistacked thin metal contacts for tandem applications“. In: *Progress in Photovoltaics: Research and Applications* 25.11 (2017), pp. 936–941. eprint: https://onlinelibrary.wiley.com/doi/abs/10.1002/pip.2919 (cit. on pp. 10, 26).

[25] J. Lee, P. Jadhav, P. D. Reusswig, et al. „Singlet Exciton Fission Photovoltaics“. In: *Accounts of Chemical Research* 46.6 (2013), pp. 1300–1311 (cit. on pp. 2, 35).

[26] M. L. Liebhaber. „Silicon heterojunction solar cells: From conventional concepts to a singlet fission multi-exciton generating hybrid approach“. PhD thesis. Freie Universität Berlin, 2017 (cit. on pp. 8, 25, 26, 33).

[27] R.E. Merrifield, P. Avakian, and R.P. Groff. „Fission of singlet excitons into pairs of triplet excitons in tetracene crystals“. In: *Chemical Physics Letters* 3.3 (1969), pp. 155–157. eprint: http://www.sciencedirect.com/science/article/pii/0009261469801223 (cit. on p. 38).

[28] K. Misiakos and D. Tsamakis. „Accurate measurements of the silicon intrinsic carrier density from 78 to 340 K“. In: *Journal of Applied Physics* 74.5 (1993), pp. 3293–3297. eprint: https://doi.org/10.1063/1.354551 (cit. on p. 11).

[29] J. Nelson. *The Physics of Solar Cells*. 5th. 57 Shelton street, London, UK: Imperial College Press, 2008 (cit. on p. 5).

[30] A. Rao and R. H. Friend. „Harnessing singlet exciton fission to break the Shockley–Queisser limit“. In: *Nature reviews materials* 2.17063 (2017). eprint: http://dx.doi.org/10.1038/natrevmats.2017.63 (cit. on pp. 1, 2).

[31] R. Santbergen, A. H. M. Smets, and M. Zeman. „Optical model for multilayer structures with coherent, partly coherent and incoherent layers“. In: *Opt. Express* 21.S2 (Mar. 2013), A262–A267. eprint: http://www.opticsexpress.org/abstract.cfm?URI=oe-21-102-A262 (cit. on p. 39).

[32] W. G. J. H. M. van Sark, A. Louwen, A. C. de Waal, B. Elsinga, and R. E. I. Schropp. „UPOT: The Utrecht Photovoltaic Outdoor Test Facility“. In: *27th European Photovoltaic Solar Energy Conference and Exhibition* (2012), pp. 3247–3249 (cit. on pp. 18, 20).

[33] O. Semonin, J. M. Luther, and M. C. Beard. „Multiple exciton generation in a quantum dot solar cell“. In: *SPIE newsroom* (2012) (cit. on pp. 1, 2, 7).

[34] W. Shockley and H. J. Queisser. „Detailed Balance Limit of Efficiency of p-n Junction Solar Cells“. In: *Journal of Applied Physics* 32.3 (1961), pp. 510–519. eprint: https://doi.org/10.1063/1.1736034 (cit. on pp. 1, 6).

[35] M. B. Smith and J. Michl. „Recent Advances in Singlet Fission“. In: *Annual Review of Physical Chemistry* 64.1 (2013), pp. 361–386. eprint: https://doi.org/10.1146/annurev-physchem-040412-110130 (cit. on pp. 3, 8).

[36] M. B. Smith and J. Michl. „Singlet Fission“. In: *Chemical Reviews* 110.11 (2010), pp. 6891–6936. eprint: https://doi.org/10.1021/cr1002613 (cit. on pp. 1, 2, 8, 38).

[37] Fraunhofer Institute for Solar Energy Systems. *Photovoltaics report*. 2018. eprint: https://www.ise.fraunhofer.de/content/dam/ise/de/documents/publications/studies/Photovoltaics-Report.pdf (cit. on p. 8).

[38] D. F. Swinehart. „The Beer-Lambert Law“. In: *Journal of Chemical Education* 39.7 (1962), p. 333. eprint: `https://doi.org/10.1021/ed039p333` (cit. on p. 12).

[39] M. Tabachnyk, B. Ehrler, S. Bayliss, R. H. Friend, and N. C. Greenham. „Triplet diffusion in singlet exciton fission sensitized pentacene solar cells“. In: *Applied Physics Letters* 103.15 (2013), p. 153302. eprint: `https://doi.org/10.1063/1.4824420` (cit. on pp. 14, 37).

[40] M. Tabachnyk, S. L. Smith, L. R. Weiss, et al. „Energy Efficient Dissociation of Excitons to Free Charges“. In: *ArXiv e-prints* (Apr. 2017). arXiv: `1704.03780 [cond-mat.mes-hall]` (cit. on p. 17).

[41] S. W. Tabernig, B. Daiber, T. Wang, and B. Ehrler. „Enhancing silicon solar cells with singlet fission: the case for Förster resonant energy transfer using a quantum dot intermediate“. In: *Journal of Photonics for Energy* 8 (2018), pp. 8–12. eprint: `https://doi.org/10.1117/1.JPE.8.022008` (cit. on pp. 2, 9).

[42] Y.P. Varshni. „Temperature dependence of the energy gap in semiconductors“. In: *Physica* 34.1 (1967), pp. 149–154. eprint: `http://www.sciencedirect.com/science/article/pii/0031891467900626` (cit. on p. 11).

[43] G. Vaubel and H. Kallmann. „Diffusion Length and Lifetime of Triplet Excitons and Crystal Absorption Coefficient in Tetracene Determined from Photocurrent Measurements“. In: *physica status solidi (b)* 35.2 (), pp. 789–792. eprint: `https://onlinelibrary.wiley.com/doi/pdf/10.1002/pssb.19690350228` (cit. on p. 14).

[44] M. W. B. Wilson, A. Rao, J. Clark, et al. „Ultrafast Dynamics of Exciton Fission in Polycrystalline Pentacene“. In: *Journal of the American Chemical Society* 133.31 (2011). PMID: 21755937, pp. 11830–11833. eprint: `https://doi.org/10.1021/ja201688h` (cit. on p. 8).

[45] M. W. B. Wilson, A. Rao, B. Ehrler, and R. H. Friend. „Singlet Exciton Fission in Polycrystalline Pentacene: From Photophysics toward Devices“. In: *Accounts of Chemical Research* 46.6 (2013), pp. 1330–1338. eprint: `https://doi.org/10.1021/ar300345h` (cit. on pp. 3, 9, 10, 25).

[46] K. Yoshikawa, H. Kawasaki, W. Yoshida, et al. „Silicon heterojunction solar cell with interdigitated back contacts for a photoconversion efficiency over 26%“. In: *Nature Energy* 2.5 (2017), p. 17032 (cit. on pp. 1, 9, 14).

List of Figures

1.1 The energy losses that lead to the SQ-limit in an ideal Si solar cell. The red part of the spectrum does not have enough energy to excite an electron to the conduction band. The blue region of the spectrum is converted into heat. In purple the effect of other extraction losses is shown. The final 33% of radiation energy is available for power conversion but the SQ-limit is reduced to 29.4% when Auger recombination is included. Figure adapted from Beard et al. [33]. 2

2.1 The singlet fission process. The picture shows the energy levels for two molecules. The molecule on the left is photo-excited to the spin-singlet S_1 state (1) and, subsequently, the energy is distributed over the two molecules; creating a spin-triplet state on each site (2). Figure adapted from Liebhaber et al. [26]. 8

2.2 Energy diagram for the essential materials in a DCT cell using pentacene as the singlet fission material and silicon as the bottom layer. 10

2.3 Measured current-voltage characteristics (circles) of a commercially available Sunpower solar cell with an efficiency of 22.5%. The model is fitted to the measurements taken under standard test conditions (AM1.5G, 1000W/m^2, 25°C). When the temperature or the irradiance is changed the model still fits the measurements with reasonable accuracy. Figure adapted from Futscher et al. [12]. 12

2.4 The transmission spectrum for a pentacene layer of 0, 100 and 500 nm in thickness when exposed to the standard AM1.5G solar spectrum. The absorption of a pentacene layer of a given thickness was calculated using the Lambert-Beer law and the absorption spectrum of a 50 nm layer of thermally evaporated pentacene. 13

2.5 The basic structure of a direct charge-transfer hybrid singlet fission device. T_1 gives the transmission to the singlet fission material to account for reflection and absorption in the top contact and hole transporting layer, T_2 gives the transmission trough the singlet fission and electron acceptor layer. 13

2.6 **(a, b)** Current density of a hybrid singlet fission solar cell (solid green lines) with a tetracene (a) and pentacene (b) layer of 500 nm calculated for a quantum efficiency of 2 and 95% transmission to the silicon wafer. The record silicon device without a singlet fission layer (black solid line). **(c, d)** The simulated efficiency of the tetracene (c) and pentacene (d) device as a function of the layer thickness and the quantum efficiency. The solid black line gives the record PCE for a silicon solar cell (26.7%). 15

2.7 The efficiency of a DCT singlet fission cell (T = 0.95) with full absorption plotted as a function of the quantum efficiency and the singlet-energy. The triplet exciton energy is set to half the singlet exciton energy. Only efficiencies greater than that of the silicon base cell (26.7%) are shown. 16

2.8 (a) The calculated efficiency of a DCT cell for QE = 1.7 and T = 0.95. (b) The available current density for the SF material and the Si layer for changing singlet exciton energy (the values have been multiplied by 1.7 and 0.95 respectively to account for the QE and T of panel (a)). In green: the open circuit voltage of the hybrid device for changing singlet exciton energy. 17

2.9 The efficiency of a DCT hybrid singlet fission cell (QE = 1.7) with perfect absorption plotted as a function of the transmission to the silicon layer and the singlet-energy. The triplet exciton energy is set to half the singlet exciton energy. Only efficiencies greater than that of the silicon base cell (26.7%) are shown. 18

2.10 The efficiency of DCT singlet fission devices for increasing quantum efficiency with a transmission of 95%. Pentacene (blue): $E_S = 1.83$ eV, $E_T = 0.86$ eV. Tetracene (orange): $E_S = 1.83$ eV, $E_T = 0.86$ eV). The other lines show the maximum efficiency reachable by varying E_S for a given QE. $E_T = \frac{1}{2} E_S$ (green), $E_T = \frac{1}{2} E_S + 100$ meV (red) and $E_T = \frac{1}{2} E_S + 200$ meV (purple). Efficiencies are given for QE = 1.7 and QE = 2.0. 19

2.11 Realistic conditions simulations of five different singlet fission materials used in hybrid devices. The temperature and spectra used for these simulations where measured in 2015 by the Utrecht Photovoltaic Outdoor Test Facility in the Netherlands [32]. (a) The efficiency of the DCT devices for silicon base cells of increasing PCE. (b,c) The efficiency of the DCT devices based on the record efficiency silicon solar cell against the average photon energy (b) and against the irradiance (c) of the measured spectra. The record silicon cell performance is given in black. The solid lines give a moving average on the data. 20

2.12 The simulated reflection from a SiN layer (70 nm) and a PEDOT:PSS(50 nm)/pentacene(100 nm) stack on a silicon wafer of infinite thickness. The calculations have been performed using a TransferMatrix model [1] and ignoring the extinction coefficient of the materials involved. . . 22
2.13 The absorbed (orange) and transmitted (blue) part of the AM1.5G solar spectrum incident on a 1000 nm tetracene layer followed by a 1000 nm pentacene layer. 24

3.1 Sketch of the solar cell concepts investigated in this work (layer thicknesses not to scale). Both devices are based on a silicon/C_{60}/pentacene stack but make use of a different hole transporting layer: PEDOT:PSS (left) and MoO_x/Al/Ag (right). 26
3.2 Current-voltage characteristics for tetracene based DCT solar cells (using the PEDOT:PSS hole-transport layer as described in figure 3.1). An increasing layer of C_{60} causes an S-shaped JV-curve which is an indication of an energy barrier in the device. Data presented with permission from M. H. Futscher. 26
3.3 Schematic setup of the QuantX-300 EQE measurement system. 29
3.4 The current-voltage characteristic of the best performing PEDOT:PSS device. 32
3.5 The EQE spectrum of the best performing PEDOT:PSS device. The reflectance as measured in the EQE setup is shown in the inset. The blue dots give the measured value, the solid orange lines give the fit to both the EQE and reflectance using the fitting parameters displayed in table 3.1. 33
3.6 The current-voltage characteristic of the Ag/Al/MoO_3 devices with 0 to 40 nm pentacene layer (left) and 60 to 100 nm pentacene layer (right). 35
3.7 The EQE spectra of the Ag/Al/MoO_3 devices with increasing pentacene layer thickness. All spectra were measured at a -1 V bias. 36
3.8 The EQE spectrum of the 60 nm pentacene Ag/Al/MoO_3 device. The reflectance as measured in the EQE setup is shown in the inset. The blue dots give the measured value, the solid orange lines give the fit to both the EQE and reflectance using the fitting parameters displayed in table 3.1. 37

List of Tables

3.1 Fitting parameters for the EQE measurement of the best PEDOT:PSS contact device. The C_{60} IQE has been set to zero since the material hardly absorbs any light and does not influence the fit. 33
3.2 Fitting parameters for the EQE measurement of the 60 nm pentacene MoO_x contact device. The C_{60} IQE has been set to zero since the material hardly absorbs any light and does not influence the fit. Obviously, metals cannot contribute to the photocurrent so their IQE has been set to zero as well. 37

Colophon

This thesis was typeset with $\LaTeX\,2_\varepsilon$. It uses the *Clean Thesis* style developed by Ricardo Langner. The design of the *Clean Thesis* style is inspired by user guide documents from Apple Inc.

Download the *Clean Thesis* style at `http://cleanthesis.der-ric.de/`.